Status: [redacted]

~~CLASSIFICATION CANCELLED~~

Copy No. 1
RM No. SA9C31

[redacted]

M. H. Rhodes 6-11-53

[redacted]

NACA

NACA change # 1493

OES

RESEARCH MEMORANDUM

for the

~~CLASSIFICATION CANCELLED~~

Bureau of Aeronautics, Navy Department

HIGH-SPEED STABILITY AND CONTROL CHARACTERISTICS OF A 0.17-SCALE MODEL OF THE McDONNELL XF2H-1 AIRPLANE

(TED No. NACA DE 318)

By John A. Axelson and Horace F. Emerson

Ames Aeronautical Laboratory
Moffett Field, Calif.

CLASSIFICATION CANCELLED

J. W. Crowley 2-25-55

NACA change # 2747

OES

Status: [redacted]

[redacted]

[redacted]

J. W. Crowley 10/10/53

NACA change # 1906

OES

NATIONAL ADVISORY COMMITTEE FOR AERONAUTICS

WASHINGTON

March 31, 1949

14

~~CLASSIFICATION CANCELLED~~

NATIONAL ADVISORY COMMITTEE FOR AERONAUTICS

RESEARCH MEMORANDUM

for the

Bureau of Aeronautics, Navy Department

HIGH-SPEED STABILITY AND CONTROL CHARACTERISTICS OF A 0.17-SCALE MODEL OF THE McDONNELL XF2H-1 AIRPLANE

(TED No. NACA DE 318)

By John A. Axelson and Horace F. Emerson

SUMMARY

High-speed wind-tunnel tests were conducted of two versions of a 0.17-scale model of the McDonnell XF2H-1 airplane to ascertain the high-speed stability and control characteristics and to study means for raising the high-speed buffet limit of the airplane. The results for the revised model, employing a thinner wing and tail than the original model, revealed a mild diving tendency from 0.75 to 0.80 Mach number, followed by a marked climbing tendency from 0.80 to 0.875 Mach number. The high-speed climbing tendency was caused principally by the pitching-moment characteristics of the wing. At 0.875 Mach number the results for the revised model indicated stick-fixed directional instability over a limited range of yaw angles, apparently caused by separated flow over the vertical tail. The test results indicate that the high-speed buffet limit of the airplane can probably be raised by reducing the thickness and changing the relative location of the horizontal and vertical tails, and by revising the inner portion of the wing to have a lower thickness-to-chord ratio and reduced trailing-edge angle. The addition of the wing-tip tanks to the revised model resulted in a forward shift in the neutral point below 0.82 Mach number.

INTRODUCTION

At the request of the Bureau of Aeronautics, Navy Department, wind-tunnel tests of a 0.17-scale model of the McDonnell XF2H-1 airplane were conducted to determine its stability and control characteristics and to devise means for raising the high-speed buffet limit of the existing experimental airplanes. The tests included the evaluation of the effects of air brakes and wing-tip tanks on the aerodynamic characteristics of the model.

This report contains the wind-tunnel results for two versions of the XF2H-1 model, designated original and revised, which represent the experimental prototypes currently being tested in flight. Since the XF2H-1 airplane was developed from the McDonnell FH-1 airplane, the results presented in references 1 and 2 for the latter served to indicate the type of stability and control difficulties likely to be encountered with the XF2H-1 airplane, although there are significant differences between the two aircraft. The wind-tunnel tests were conducted through a Mach number range from 0.40 to 0.90, corresponding to a Reynolds number range from 3,200,000 to 5,100,000. The results of the tests herein reported served as a basis for making additional modifications to the model.

SYMBOLS

The axes used for the presentation of the data with an indication of the directions of the positive forces and moments are presented in figure 1. The coefficients and symbols are defined as follows:

C_D drag coefficient $\left(\frac{\text{drag}}{qS}\right)$

C_L lift coefficient $\left(\frac{\text{lift}}{qS}\right)$

C_Y side-force coefficient $\left(\frac{\text{side force}}{qS}\right)$

C_h hinge-moment coefficient $\left(\frac{\text{hinge moment}}{2qM_A}\right)$

C_l rolling-moment coefficient about the fuselage reference axis $\left(\frac{\text{rolling moment}}{qSb}\right)$

C_m	pitching-moment coefficient about the airplane lateral axis through the quarter-chord point of the mean aerodynamic chord $\left(\dfrac{\text{pitching moment}}{qS\bar{c}}\right)$
C_n	yawing-moment coefficient about the vertical airplane axis passing through the intersection of the pitching moment and the fuselage reference axes $\left(\dfrac{\text{yawing moment}}{qSb}\right)$
H	total pressure, pounds per square foot
M	Mach number
M_A	moment about hinge line of control-surface area behind the hinge line, feet cubed
P	pressure coefficient $\dfrac{\text{(local static pressure)}-\text{(free-stream static pressure)}}{q}$
P_{cr}	critical pressure coefficient, corresponding to local sonic velocity
S	wing area, square feet
V	velocity, feet per second
W	airplane weight, pounds
b	wing span, feet
c	local chord, feet
$\bar{c}$	wing mean aerodynamic chord $\left(\dfrac{\int_0^{b/2} c^2\,dy}{\int_0^{b/2} c\,dy}\right)$, feet
i	incidence, degrees
q	dynamic pressure $\left(\frac{1}{2}\rho V^2\right)$, pounds per square foot
t/c	thickness-to-chord ratio
y	lateral coordinate, measured from plane of symmetry, feet
α	angle of attack of fuselage reference line, degrees

δ control-surface deflection, degrees

ρ free-stream mass density, slugs per cubic foot

ψ angle of yaw, degrees

Subscripts

a aileron

e elevator

r rudder

t horizontal tail

u uncorrected

APPARATUS AND TESTS

Model Description

The XF2H-1 airplane is a single-place, shipboard fighter powered by two 24-inch Westinghouse turbojet engines housed in the enlarged wing-fuselage fillets. A three-view drawing of the model appears in figure 2. The pertinent dimensions of the two model versions are shown in table I, the major differences being in the airfoil sections of the wings and tails. Figure 3 compares the geometrical characteristics of the wings for the original and revised models.

Auxiliary devices tested include a separate set of air brakes for each model version and wing-tip tanks on the revised model. For both model versions, the flow of air through the ducts provided an inlet-velocity ratio of 0.35 at all Mach numbers.

Support System

The 0.17-scale XF2H-1 model was mounted in the Ames 16-foot high-speed wind tunnel on the sting-support system shown in figure 4, the sting having a diameter of 4 inches. The wind-tunnel test section was not circular, but had vertical flats which reduced the width to 12 feet, resulting in a total cross-sectional area of 172 square feet. The aerodynamic forces and moments on the model were measured by means of an electrical strain-gage balance mounted on the upstream end of the sting and housed within the model fuselage. The sting-support system was so arranged that the moment center of the model remained on the horizontal center line of the wind tunnel when the angle of attack was varied. Yawing of the model was accomplished with the model rotated 90° on the sting, the pitching motion of the sting providing yawing motion to the model. During the yaw tests, the model was at zero angle of attack.

Tests

Lift, drag, and pitching moment were measured for the original and revised models. In addition, side force and yawing moment were measured for the revised model. Aileron, rudder, and elevator hinge moments were measured on the revised model using resistance-type electrical strain gages.

Pressure distributions were measured on the wing and tail of the revised model for evaluating minimum pressure locations and critical Mach numbers. A rake was mounted on the horizontal tail of the model to determine the location of the wing wake. Rakes were placed in the duct and at the duct exit for measuring the velocity in the duct and the internal drag.

PRESENTATION OF DATA

Corrections

Jet-boundary and blockage corrections calculated by the methods given in references 3 and 4, respectively, have been applied to the data. The jet-boundary corrections were

$$\Delta\alpha = 0.41\ C_L,\ \text{deg}$$

$$\Delta C_D = 0.0071\ C_L^2$$

$$\Delta C_m = 0.0054\ C_L\ \text{(tail-on data only)}$$

The test Mach numbers corrected and uncorrected for blockage were as follows:

Uncorrected	.399	.598	.697	.746	.771	.795	.818	.840	.862	.882
Corrected	.400	.600	.700	.750	.775	.800	.825	.850	.875	.900

The test Mach numbers were maintained within ± 1 percent of the indicated values. The angle of attack was held within $\pm 0.1^{\circ}$.

A drag coefficient of 0.0020, representing the internal drag of the ducts in the model, was subtracted from all drag results. This value was determined from a survey of the total and static pressures at the duct exit and remained constant throughout the Mach number range. No corrections have been applied to account for the effects of the sting, fairing, or base pressure.

Order of Presentation of Data

The basic force data for both model versions are presented in figures 5 through 11, while figures 12 and 13 compare the aerodynamic characteristics of the two models. The effects of wing-tip tanks on the aerodynamic characteristics of the revised model are presented in figure 14. The longitudinal control characteristics of the revised model are shown in figure 15, while figure 16 presents the directional stability characteristics. Figure 17 presents the rudder and aileron characteristics of the revised model.

Several pictures of tufts indicating the flow over both model versions are presented in figures 18 and 19. The spanwise distribution of critical Mach number for the revised wing and the critical Mach numbers for the revised tail are shown in figure 20. Wing wakes measured at the horizontal tail for four different Mach numbers and angles of attack are presented in figure 21.

RESULTS AND DISCUSSION

Basic Force and Pitching-Moment Data

Effect of model revisions.- The polars and lift curves for the original and revised models with and without tail surfaces are presented in figures 5 and 6. It may be seen that the shift in the angle of attack for zero lift with increasing Mach number was considerably reduced by revising the wing. A corresponding improvement may be noted in the pitching-moment curves of figures 7(a) and 7(b), where the increase in pitching-moment coefficients for constant lift coefficients above 0.80 Mach number became less pronounced for the revised model.

Air brakes.- The variations of pitching-moment coefficient with lift coefficient for the original model with and without air brakes for two stabilizer settings are shown in figure 8. With the air brakes extended and with the negative stabilizer setting, the model was unstable at 0.775 Mach number up to a lift coefficient of 0.45 as shown in figure 8(b).

The variation of pitching-moment coefficient with lift coefficient for the revised model with air brakes is presented in figure 9 for two elevator settings. The static longitudinal stability was neutral at 0.75 Mach number in the lift-coefficient range from 0.2 to 0.5.

Wing-tip tanks.- The variations of drag and pitching-moment coefficients with lift coefficient for the revised model with wing-tip tanks are presented in figure 10. The static longitudinal stability was neutral at 0.7 Mach number from 0.3 lift coefficient to 0.6 lift coefficient.

Elevator characteristics for the revised model.- The variation of pitching-moment coefficient with lift coefficient at several Mach numbers for the revised model with a stabilizer setting of 1° is shown in figures 11(a) through 11(h). Superimposed on the pitching-moment curves are the variations of elevator hinge-moment coefficient with lift coefficient. The static longitudinal stability decreased with increasing Mach number up to a Mach number of 0.80, where the curves assumed an S-shape, the variation with lift coefficient increasing at the higher Mach numbers. At the lower Mach numbers there was little variation in the elevator hinge-moment coefficient with angle of attack, but above 0.80 Mach number the variation increased and became nonuniform.

Variations with Mach Number of Lift, Drag, and Pitching-Moment Characteristics

Effect of model revisions.- The variations with Mach number of the drag coefficients for the two models with and without air brakes are shown in figure 12. The drag of the revised model without air brakes was less than that of the original model except at zero lift below 0.65 Mach number where the drags were equal. The revised model possessed the higher Mach number for drag divergence.

A summary of the aerodynamic parameters of the two model versions is presented in figure 13. The Mach number of lift divergence and the lift-curve slope were increased as a result of the model revisions, as shown in figures 13(a) and 13(b). The increase in the Mach number for lift divergence was approximately 0.04, while the increase in the lift-curve slope varied between 5 and 19 percent, depending on the Mach number. As shown in figure 13(c), the change with Mach number of the angle of attack for zero lift was reduced from 2.3° to 1.2° by the model revisions. This improvement in zero-lift angle was noted previously in the discussion of figure 6. The maximum lift-to-drag ratio was higher for the revised model throughout the entire Mach number range of the tests as shown in figure 13(d), the increase varying from 2.5 at 0.4 Mach number to 1.5 at the higher Mach numbers.

The static longitudinal stability of each model version expressed as the location of the stick-fixed neutral point evaluated at a lift coefficient of 0.1 is shown in figure 13(e). For both models, minimum static longitudinal stability occurred between 0.70 and 0.80 Mach number, the stick-fixed neutral points occurring as far forward as 27 percent of the wing mean aerodynamic chord. The changes in stability with increasing Mach number were caused principally by the changes in wing lift-curve slope and downwash at the tail. A discussion of the factors affecting static longitudinal stability at high subsonic Mach numbers is presented in reference 5.

The variations in pitching-moment coefficient with Mach number for the two models with and without tail surfaces are shown in figures 13(f) and 13(g). The large increases in pitching-moment at the higher Mach numbers already noted in figure 7 and shown in detail in figure 13(f) for the models with the tails removed are reflected in the pitching-moment curves of figure 13(g) for the complete models. The marked pitch-up tendency encountered during the flight tests of the prototype airplanes are borne out in the wind-tunnel results. This phenomenon was shown in references 2 and 5 to be a characteristic of the section of the wing.

The stabilizer and elevator effectiveness for the two model versions at a model lift coefficient of 0.2 are shown in figures 13(d) and 13(i). The stabilizer effectiveness was determined from tests covering a range of stabilizer settings from -1° to 2°. The progressive reduction in effectiveness of the horizontal tail components above about 0.75 Mach number may be partially attributed to the interference resulting from the near coincidence of the locations of the minimum pressures over the horizontal and vertical tails. As shown in figure 21, there was no reduction in dynamic pressure at the horizontal tail. Figure 13(j) presents the variation with Mach number of the elevator hinge-moment parameter $(\partial C_{h_e}/\partial \delta_e)_{C_L}$, the results indicating an increase in the parameter above 0.78 Mach number.

Air Brakes.- The variations of drag coefficient with Mach number for the two models with air brakes are shown in figure 12(b). It should be repeated that the air brakes tested on the two model versions differed considerably, as described in table I, thereby accounting for the large differences in drag. The air brakes on the revised model were tested with and without perforations, but no measurable differences appeared in the results.

Wing-tip tanks.- The maximum lift-to-drag ratios, lift-curve slopes, and stick-fixed neutral points are shown in figure 14 for the revised model with and without wing-tip tanks. It should be noted that below 0.80 Mach number there was practically no variation in elevator hinge-moment coefficient with model angle of attack, therefore the variation of stick-free neutral points with Mach number would follow very closely the stick-fixed results given in figure 14(b). Although the lift-curve slope was increased by the end-plate effects of the tanks, the increased drag resulted in a slight reduction of the maximum lift-to-drag ratio. The tanks had a slightly destabilizing effect at most of the Mach numbers, moving the neutral point as far forward as the 26-percent point of the mean aerodynamic chord at 0.73 Mach number.

Longitudinal trim and control characteristics.- Figure 15 presents the trim lift coefficient and the elevator deflections and longitudinal-control forces for level flight evaluated from the results for the revised model. As shown in figure 15(a), the model trimmed at positive lift coefficients throughout the entire Mach number range of tests. Figures 15(b) and 15(c) show the calculated elevator angles and control forces for level flight of the XF2H-1 airplane at altitudes of 15,000 and 30,000 feet with a gross weight of 14,700 pounds and the center of gravity at the quarter point of the mean aerodynamic chord. A mild nosing-down tendency is indicated from 0.75 to 0.80 Mach number, followed by a marked pitching-up tendency above 0.80 Mach number which was indicated in the pitching-moment curves of figure 13(g) and the trim lift coefficients shown in figure 15(a).

Directional stability characteristics.- The side-force, rolling-moment, and yawing-moment parameters for the revised model in yaw are presented in figure 16. The yawing-moment results indicate static directional instability at 0.875 Mach number with zero rudder deflection for a limited range of yaw angles.

Rudder and aileron characteristics.- The rudder and aileron characteristics of the revised model are presented in figure 17. The negative value of the rudder-effectiveness parameter shown in figure 17(a) decreased with increasing Mach number due to the separation shown in the tuft pictures of figure 19. The aileron-effectiveness parameter, shown in figure 17(e), decreased abruptly at 0.78 Mach number as a result of the separation which progressed outward over the after portion of the wing at the higher Mach numbers. The increase in the negative value of the aileron hinge-moment parameter above 0.75 Mach number shown in figure 17(f) was probably caused by changes in the separation accompanying aileron deflection.

Pressure Distribution and Tuft Studies

Wing.- Both the original and the revised models had favorable stall patterns at 0.40 Mach number and 12° angle of attack with no early tip or root stall, as shown in the tuft pictures in figures 18 and 19. Tuft pictures are presented for the original model at Mach numbers of 0.40 and 0.825 in figure 18. The pictures in figure 19 are of the revised model for Mach numbers of 0.40, 0.825, and 0.875. The buffet limit of the prototype airplanes determined from flight tests was approximately 0.825. The tuft pictures of the models show rough flow emanating from the tail intersections and marked separation from the wings at 0.825 Mach number, thus locating the regions of separation which lead to buffeting. The separation from the wing probably is the major cause of the buffet because of the relatively large area affected.

On the basis of the spanwise variation of wing critical Mach number shown in figure 20(a) and of wing thickness and trailing-edge angle shown in figure 3, it appears that the buffet limit can be raised by modifying the inner portion of the wing so that the trailing-edge angle and thickness-to-chord ratio are reduced. Such modifications would tend to raise the buffet limit and delay the development of the pitch-up moment of the wing to a higher Mach number. (See fig. 13(f).)

Tail.- The separation at the intersection of the horizontal and vertical tails, evident in the tuft pictures, may be attributed to the relatively low critical Mach number of 0.69 for the intersection as indicated by the results presented in figure 20. The separation at the intersection began at a Mach number of about 0.75 and increased in intensity at the higher Mach numbers. It appears that the flow at the intersection can be improved by displacing the maximum thickness of the horizontal and vertical tails as far apart as practicable and by reducing the thickness of both tail planes.

Results of wake surveys at the horizontal tail are presented in figure 21, the wing wake total-pressure decrement being plotted relative to the position of the horizontal tail plane. The results indicate that the tail was above the wing wake at all test Mach numbers and angles of attack.

CONCLUSIONS

The principal conclusions drawn from high-speed wind-tunnel tests of two versions of a 0.17-scale model of the XF2H-1 airplane were as follows:

1. The results for the revised model indicated a mild pitching-down tendency between 0.75 and 0.80 Mach number, followed by a marked pitching-up tendency above 0.80 Mach number. No other unusual control tendencies were noted.

2. At 0.875 Mach number the results for the revised model indicated static directional instability over a limited range of yaw angles.

3. Although the revised model possessed static longitudinal stability characteristics which were superior to those of the original model, further modifications appear desirable to improve the high-speed longitudinal and directional stability and to raise the buffet limit.

4. The proposed modifications to the model for alleviating the undesirable stability characteristics and raising the buffet limit include reducing the trailing-edge angle and thickness-to-chord ratio of the inner portion of the wing and reducing the thickness of the horizontal and vertical tail planes, as well as displacing the maximum thickness of the two units as far apart as practicable.

5. The addition of the wing-tip tanks to the revised model resulted in a forward displacement of the neutral point below 0.82 Mach number.

Ames Aeronautical Laboratory,
National Advisory Committee for Aeronautics,
Moffett Field, Calif.

REFERENCES

1. Axelson, John A., and Eley, Herman O.: High Speed Longitudinal Stability and Control of the McDonnell XFD-1 Airplane with Sealed Internally Balanced Elevators as Predicted from Wind-Tunnel Tests (TED No. NACA 2310). NACA MR No. A5K23, 1945.

2. Axelson, John A., and Eley, Herman O.: Effects of Mach number on the Spanwise Load Distribution and Aerodynamic Characteristics of the Wing of the McDonnell XFD-1 Airplane Predicted from Wind-Tunnel Tests (TED No. 2310). NACA ~~RM~~ MR No. A6A23, 1946.

3. Silverstein, Abe, and White, James A.: Wind-Tunnel Interference with Particular Reference to Off-Center Positions of the Wing and to the Downwash at the Tail. NACA Rep. No. 547, 1936.

4. Herriot, John G.: Blockage Corrections for Three-Dimensional Flow Closed-Throat Wind Tunnels with a Consideration of the Effect of Compressibility. NACA RM No. A7B28, 1947.

5. Axelson, John A.: Longitudinal Stability and Control of High-Speed Airplanes with Particular Reference to Dive Recovery. NACA RM No. A7C24, 1947.

TABLE I.– GEOMETRIC CHARACTERISTICS OF THE 0.17–SCALE XF2H–1 MODELS

	Original Model	Revised Model
Wing		
Area, sq ft	8.36	8.53
Span, ft	7.060	7.076
Mean aerodynamic chord, ft	1.250	1.252
Aspect ratio	5.96	5.89
Taper ratio	0.448	0.520
Geometric twist, deg	0	0
Dihedral, deg	6	3
Incidence, deg	–0.5	–0.5
Theoretical root section, leading and trailing edges of outer wing panel extended	NACA 66(215) –213(a=0.6) at wing station 0	NACA 65–212 (a=1.0) at wing station 15.0
Theoretical tip section	NACA 66(215) –213(a=0.6)	NACA 63–209 (a=1.0)

Aileron	
Type	Flat sides, radius nose, sealed
Area aft of hinge line (one aileron), sq ft	0.272
Hinge–line length, ft	1.252
Area moment about hinge line, ft^3	.0243
Aileron hinge–line location, percent wing chord	76

	Original Model	Revised Model
Horizontal tail		
Area, sq ft	2.00	2.02
Span, ft	3.06	3.06
Aspect ratio	4.68	4.65
Taper ratio	.603	.603
Incidence, deg	0	1
Dihedral, deg	4	0
Section	NACA 65-012	NACA 65-011
Tail length (0.25 $\bar{c}$ wing to 0.25 $\bar{c}$ tail), wing $\bar{c}$	2.32	2.30
Elevator		
Type	Flat sides, radius nose, unsealed	Flat sides, radius nose, unsealed
Area aft of hinge line (one elevator), sq ft	0.270	0.255
Span (one elevator), ft	1.380	1.333
Area moment about hinge line, ft^3	.0282	.0242
Horn area, sq ft	0	.0151
Elevator hinge-line location, percent chord	70	70
Average trailing-edge angle, deg	13	12

	Original Model	Revised Model
Vertical tail		
Area, sq ft	1.12	1.11
Span, ft	1.217	1.219
Aspect ratio	1.27	1.34
Taper ratio	0.452	0.453
Section	NACA 65-012	NACA 65-011
Rudder		
Type		Flat sides, radius nose, unsealed
Area aft of hinge line, sq ft		0.293
Span, ft		1.219
Area moment about hinge line, ft^3		0.0362
Average trailing-edge angle, deg		13
Air brakes		
Total frontal area, sq ft	0.173	0.335
Height from wing surface, in.		
Upper	0.96	1.90
Lower	1.07	1.90
Chordwise location, percent wing chord	72.3	71.6
Spanwise location of inboard end of brake, percent wing semispan	48.5	36.8

	Original Model	Revised Model
Tip tanks		
Frontal area (one tank), sq ft		0.0953
Length, ft		2.58
Fineness ratio		7.4

FIGURE LEGENDS

Figure 1.– Axes and positive directions of forces, moments, and deflections.

Figure 2.– Three-view drawing of the 0.17-scale model of the XF2H-1 airplane.

Figure 3.– Geometric characteristics of the wing for the original and revised model.

Figure 4.– The 0.17-scale XF2H-1 model mounted on the sting-support system in the Ames 16-foot high-speed wind tunnel. (a) Model upright with wing-tip tanks. (b) Model inverted.

Figure 5.– Drag polars for the original and revised models at various Mach numbers. (a) Original model, less tail. (b) Original model.

Figure 5.– Concluded. (c) Revised model, less tail. (d) Revised model.

Figure 6.– Lift curves for the original and revised models at various Mach numbers. (a) Original model, less tail. (b) Revised model, less tail.

Figure 6.– Concluded. (c) Original model. (d) Revised model.

Figure 7.– Variation of pitching-moment coefficient with lift coefficient at various Mach numbers for the original and revised models, with and without tail surfaces. (a) Original model, less tail. (b) Revised model, less tail.

Figure 7.– Concluded. (c) Original model, i_t, 0°. (d) Revised model. i_t, 1°.

Figure 8.– Effect of Mach number and stabilizer incidence on the variation of pitching-moment coefficient with lift coefficient for the original model, with and without air brakes. Elevators neutral. (a) Original model. (b) Original model with air brakes.

Figure 9.– Variation of pitching-moment coefficient with lift coefficient at various Mach numbers for the revised model with air brakes. (a) δ_e, 0°. (b) δ_e, 4°.

Figure 16.– Variation with Mach number of the directional-stability parameters for the revised model. α, 0°, δ_r, 0°. (a) Side-force parameter. (b) Rolling-moment parameter. (c) Yawing-moment coefficient.

Figure 17.– Variation with Mach number of several rudder and aileron parameters for the revised model. (a) Rudder-effectiveness parameter. (b) Rudder side-force parameter. (c) Rudder rolling-moment parameter. (d) Rudder hinge-moment parameter. (e) Aileron-effectiveness parameter. (f) Aileron hinge-moment parameter.

Figure 18.– Tufts on the original model. (a) Plan view. M, 0.40; α_u, 0°; C_L, 0.08. (b) Side view. M, 0.40; α_u, 0°; C_L, 0.08. (c) Plan view. M, 0.40; α_u, 12°; C_L, 1.01. (d) Side view. M, 0.40; α_u, 12°; C_L, 1.01.

Figure 18.– Concluded. (e) Plan view. M, 0.825; α_u, 0°; C_L, –0.08. (f) Side view. M, 0.825; α_u, 0°, C_L, –0.08. (g) Plan view. M, 0.825; α_u, 4°; C_L, 0.26. (h) Side view. M, 0.825; α_u, 4°; C_L, 0.26.

Figure 19.– Tufts on the revised model. (a) Plan view. M, 0.40; α_u, 0°; C_L, 0.05. (b) Side view. M, 0.40; α_u, 0°; C_L, 0.05. (c) Plan view. M, 0.40; α_u, 12°; C_L, 0.99. (d) Side view. M, 0.40; α_u, 12°; C_L, 0.99.

Figure 19.– Continued. (e) Plan view. M, 0.825; α_u, 0°; C_L, 0.03. (f) Side view. M, 0.825; α_u, 0°; C_L, 0.03. (g) Plan view. M, 0.825; α_u, 4°; C_L, 0.36. (h) Side view. M, 0.825; α_u, 4°; C_L, 0.36.

Figure 19.– Concluded. (i) Plan view. M, 0.875; α_u, 2°; C_L, 0.08. (j) Side view. M, 0.875; α_u, 2°; C_L, 0.08. (k) Plan view. M, 0.875; α_u, 6°; C_L, 0.3 (estimated) (l) Side view. M, 0.875; α_u, 6°; C_L, 0.3 (estimated).

Figure 20.– Experimentally determined critical Mach number for the revised model. (a) Spanwise variation of critical Mach number for wing. (b) Variation with Mach number of minimum pressure coefficient for the tail. Model lift coefficient, 0.2.

Figure 21.– Wing wake at leading edge of the horizontal tail measured at stabilizer station 6.3 inches. (a) α, 12°; M, 0.317. (b) α, 8°; M, 0.726. (c) α, 4°; M, 0.829. (d) α, 4°; M, 0.872.

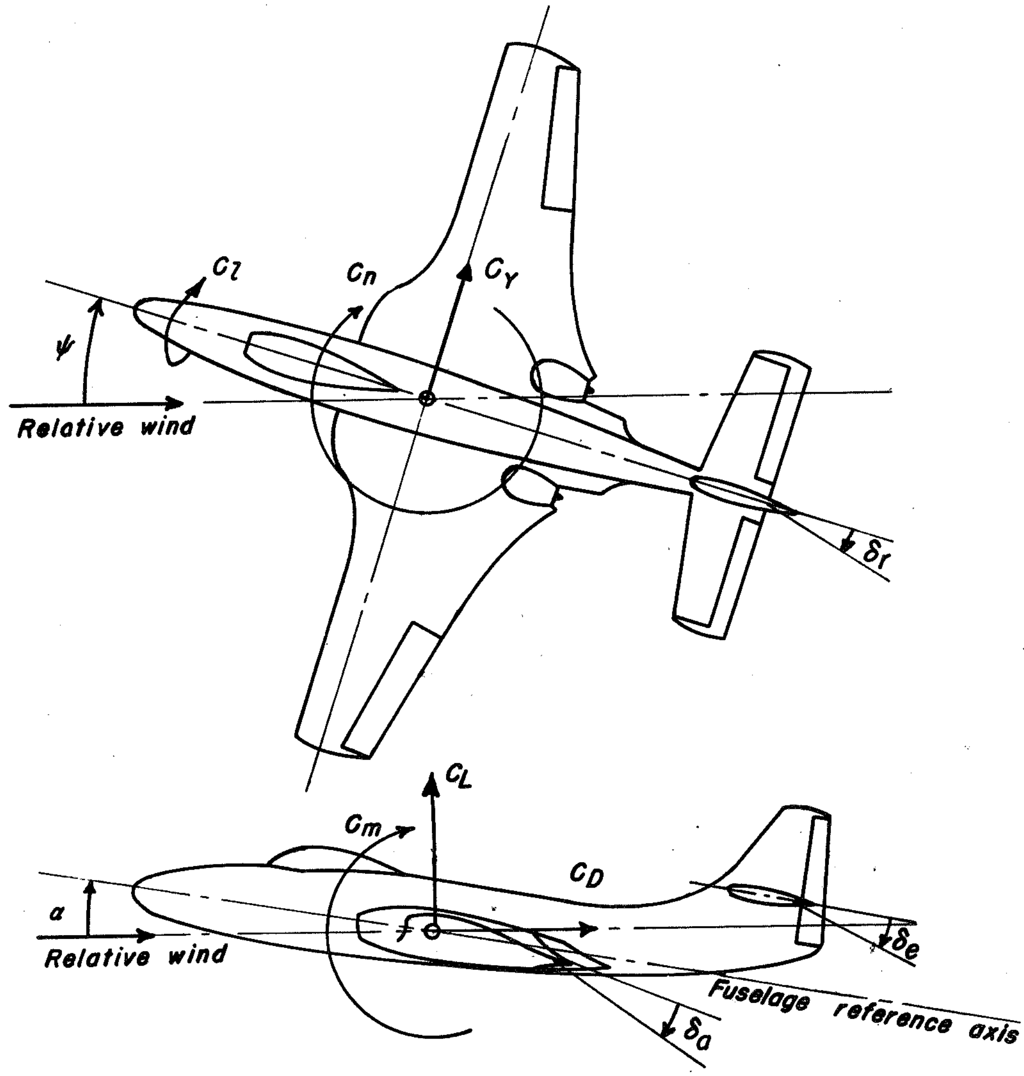

Figure 1.– Axes and positive directions of forces, moments, and deflections.

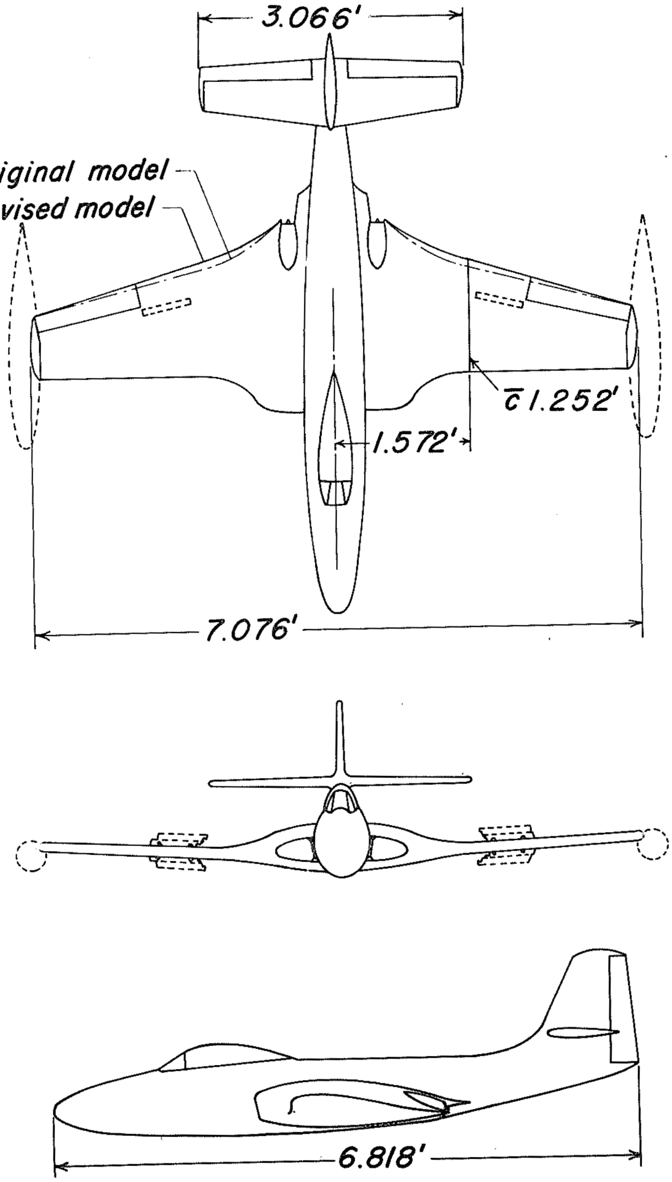

Figure 2.- Three-view drawing of the 0.17-scale model of the XF2H-1 airplane.

NATIONAL ADVISORY COMMITTEE FOR AERONAUTICS

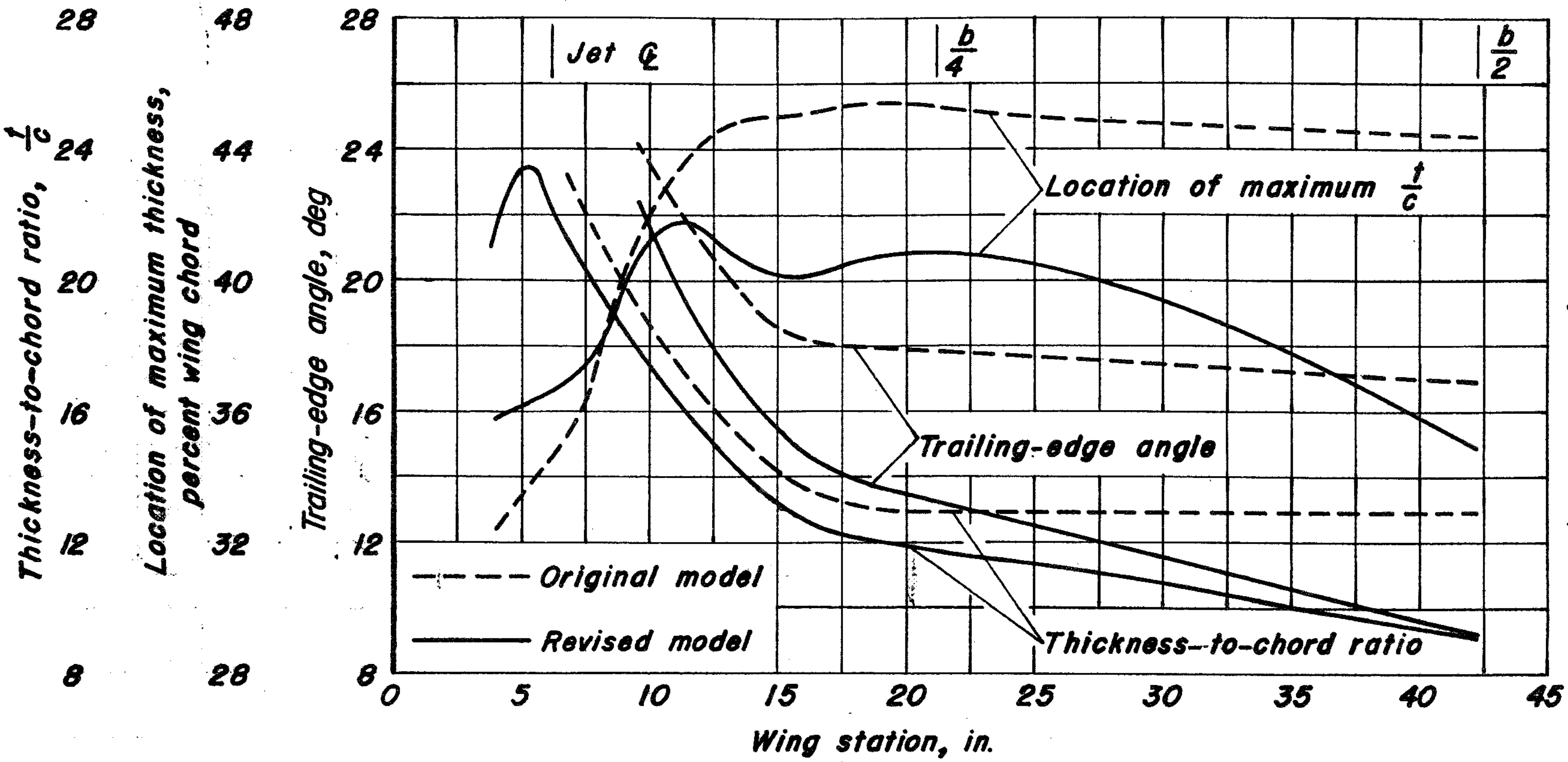

Figure 3.- Geometric characteristics of the wing for the original and revised model.

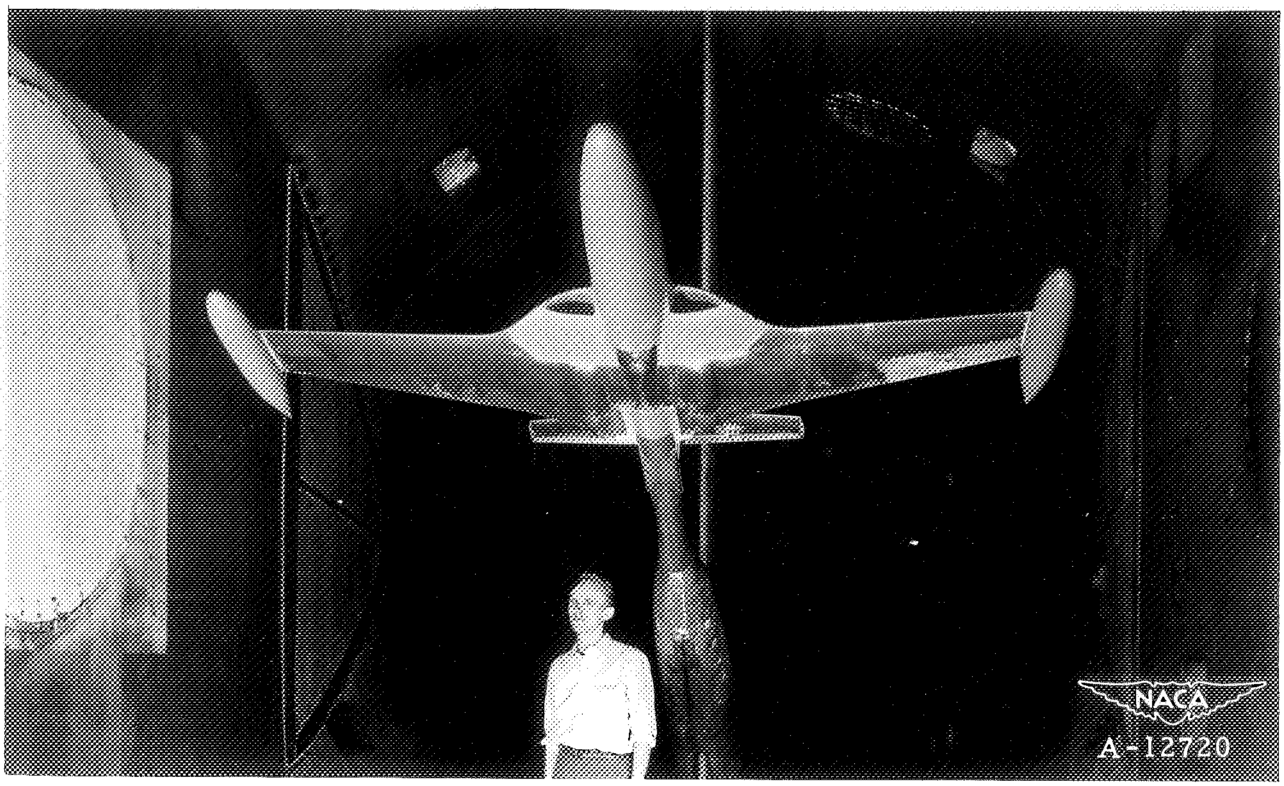

(a) Model upright with wing-tip tanks.

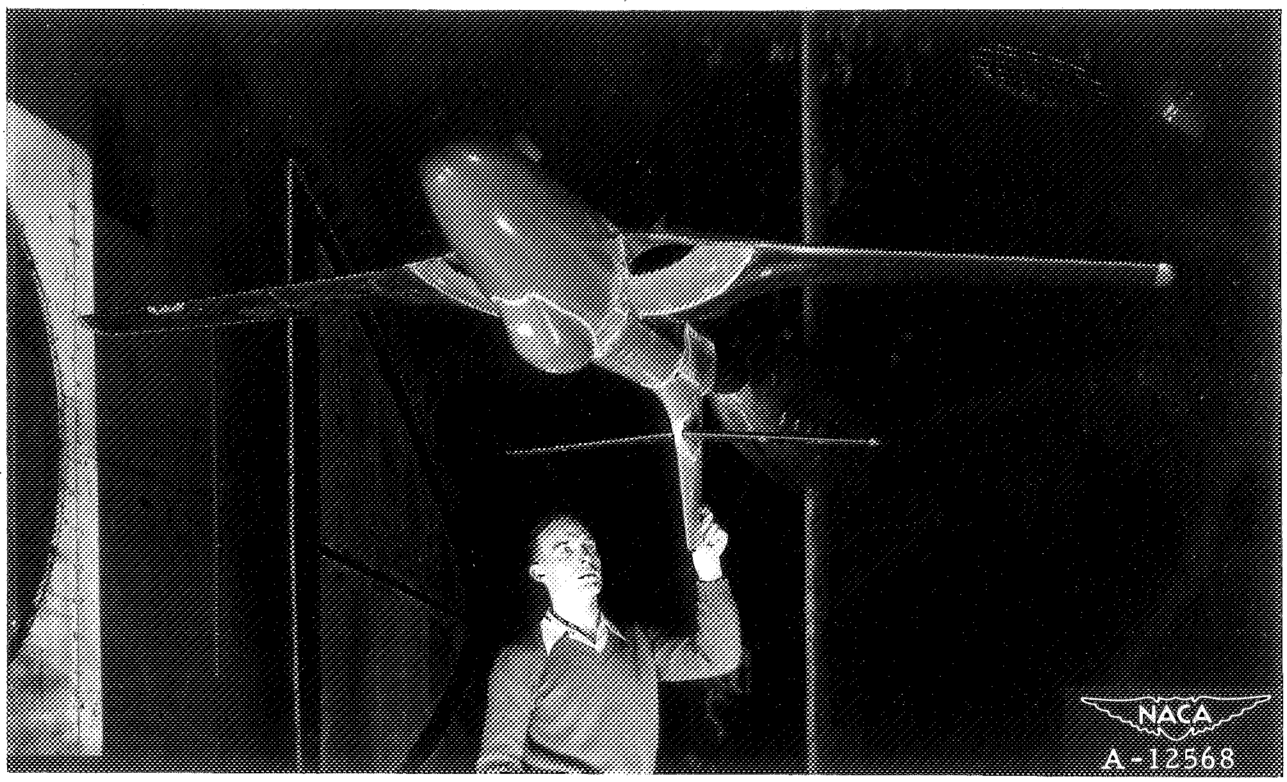

(b) Model inverted.

Figure 4.– The 0.17-scale XF2H-1 model mounted on the sting-support system in the Ames 16-foot high-speed wind tunnel.

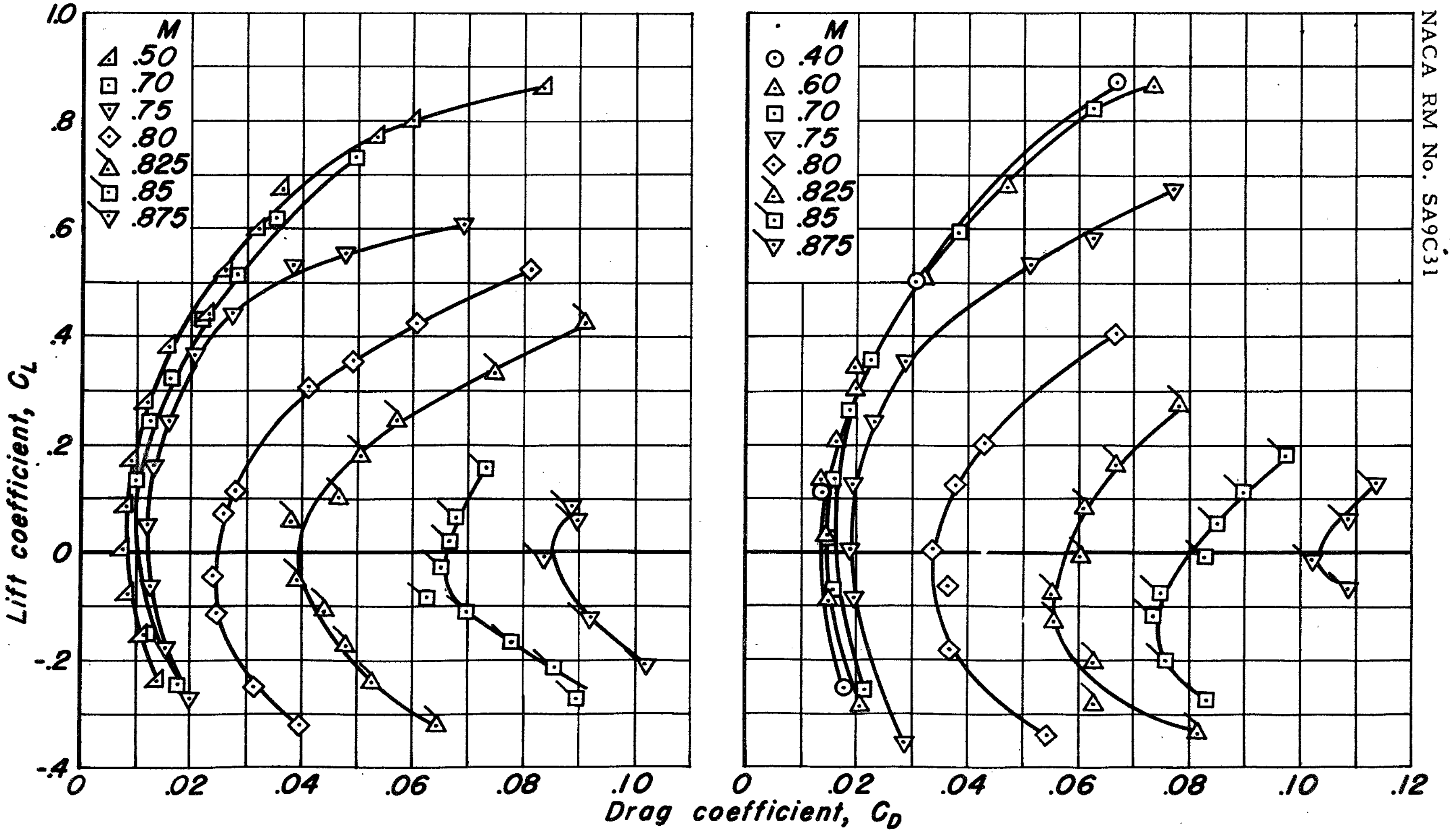

(a) Original model, less tail.

(b) Original model.

Figure 5.– Drag polars for the original and revised models at various Mach numbers.

CONFIDENTIAL

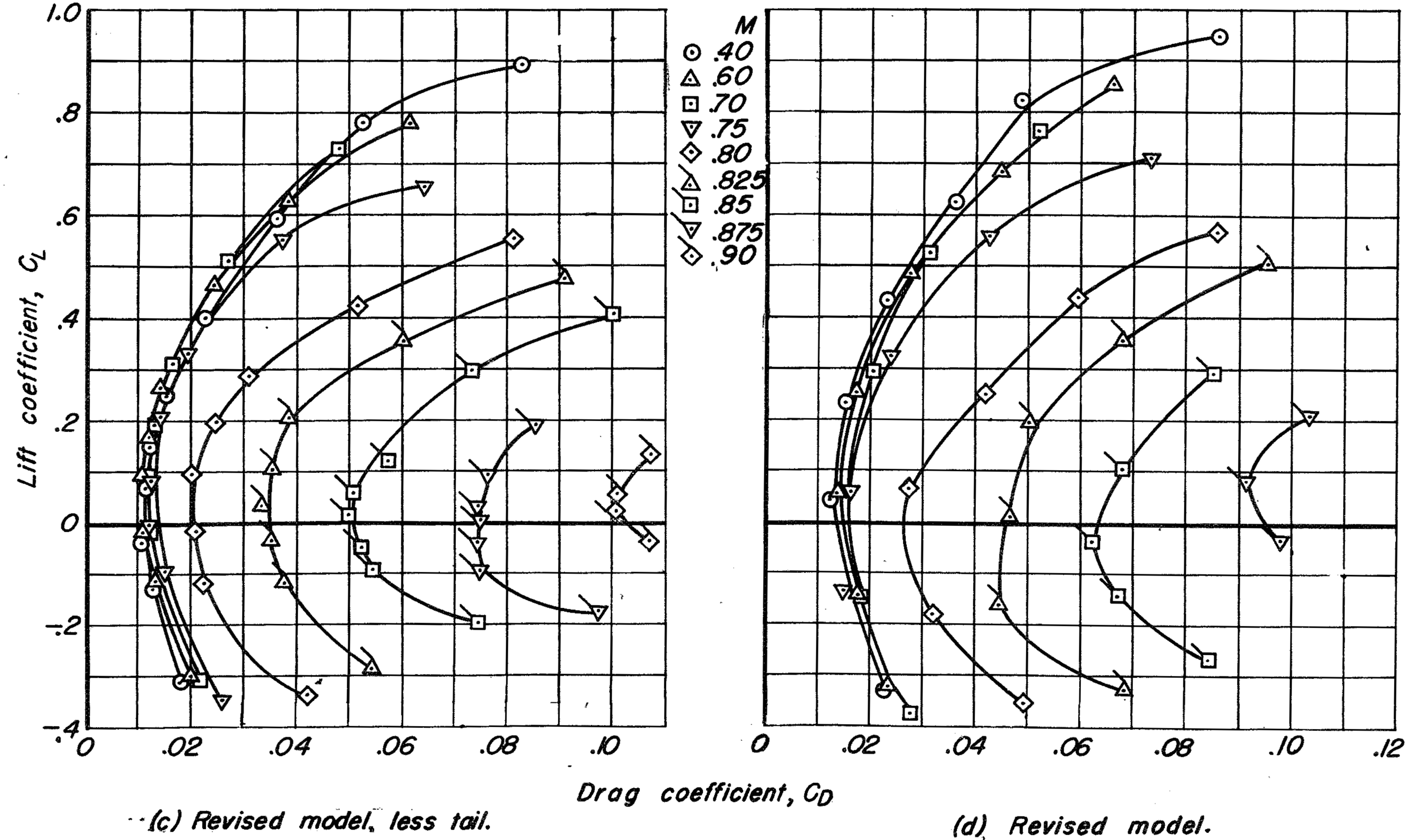

Figure 5.– Concluded.

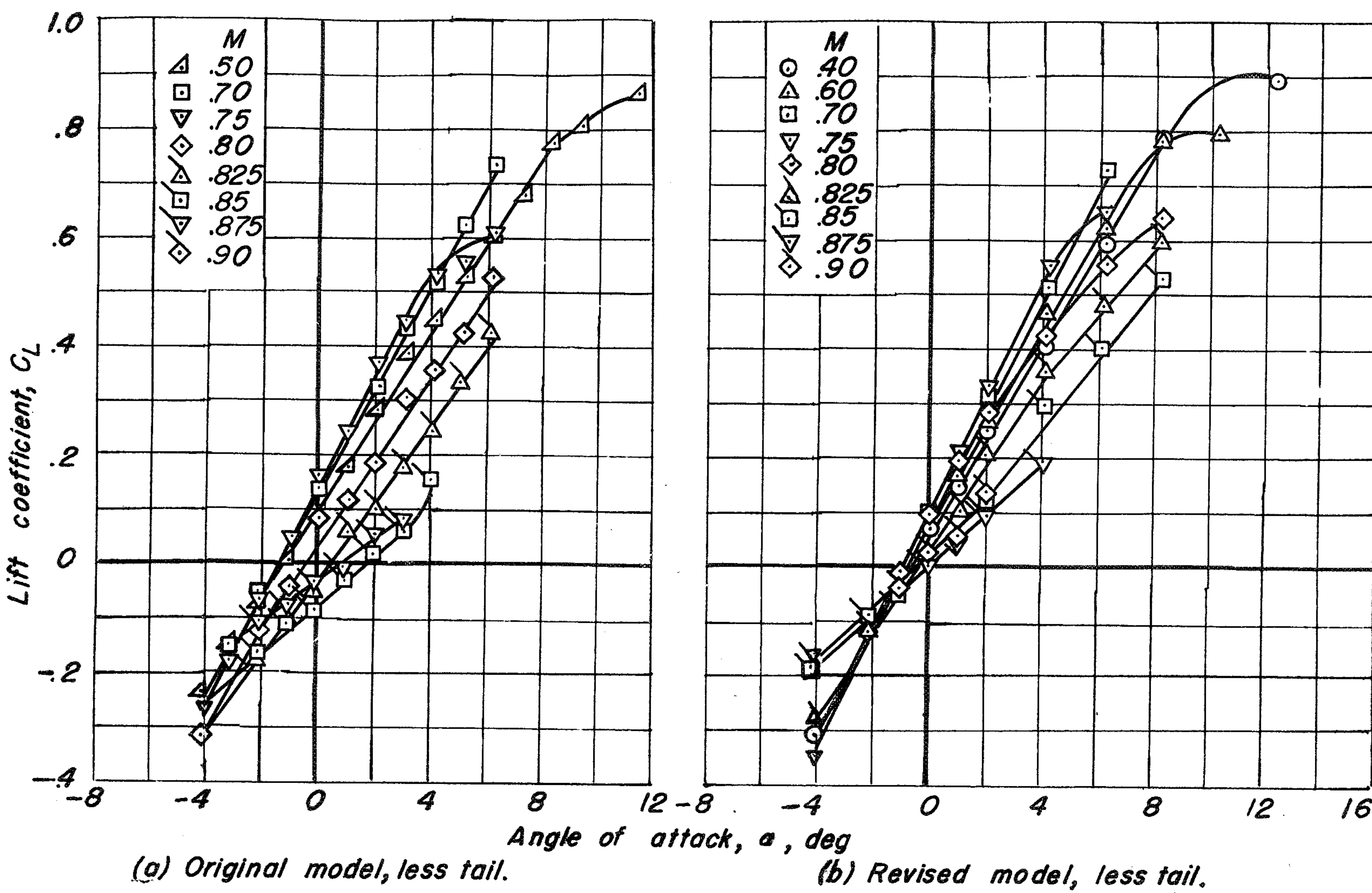

Figure 6.- Lift curves for the original and revised models at various Mach numbers.

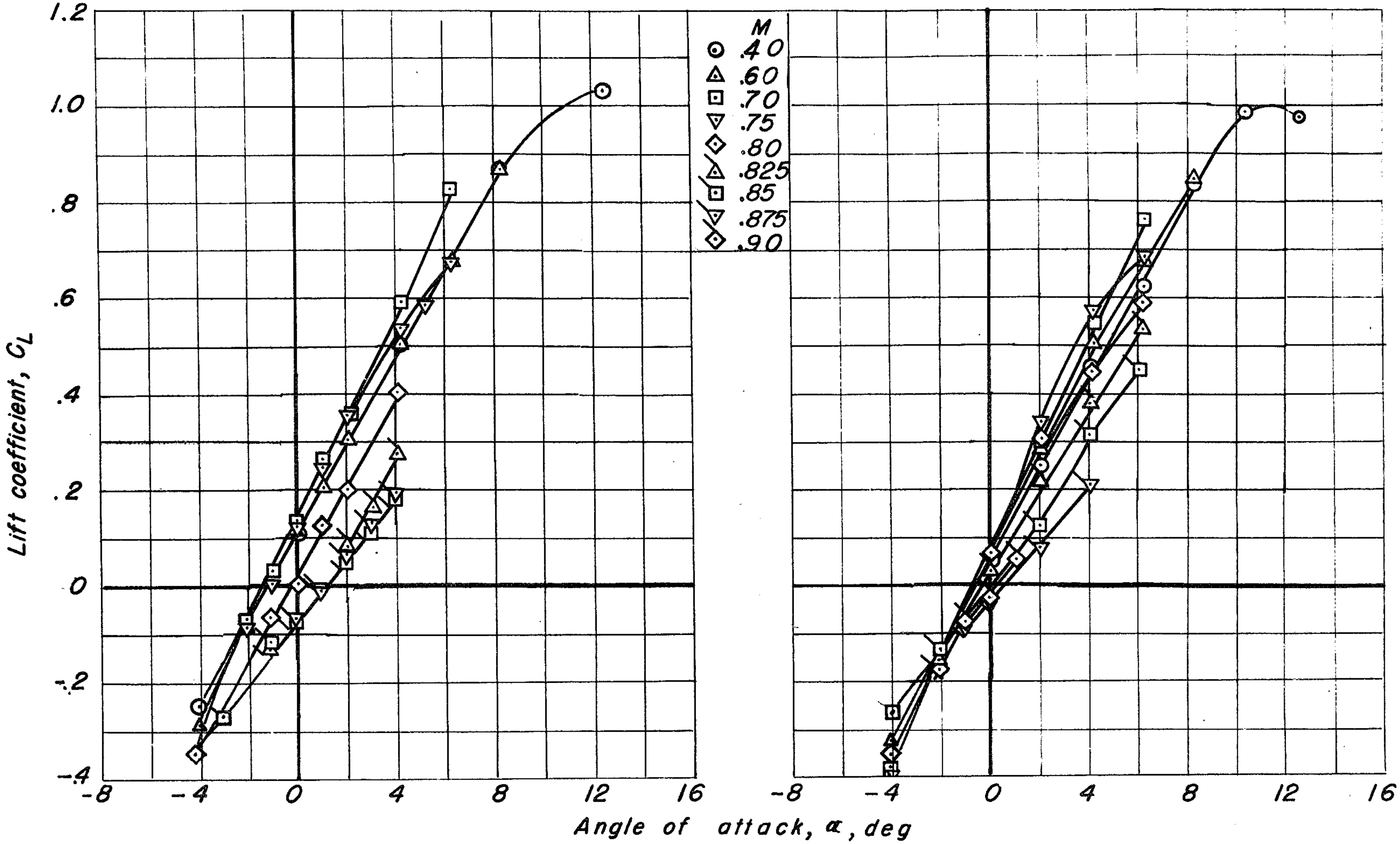

(c) Original model.

(d) Revised model.

Figure 6.- Concluded.

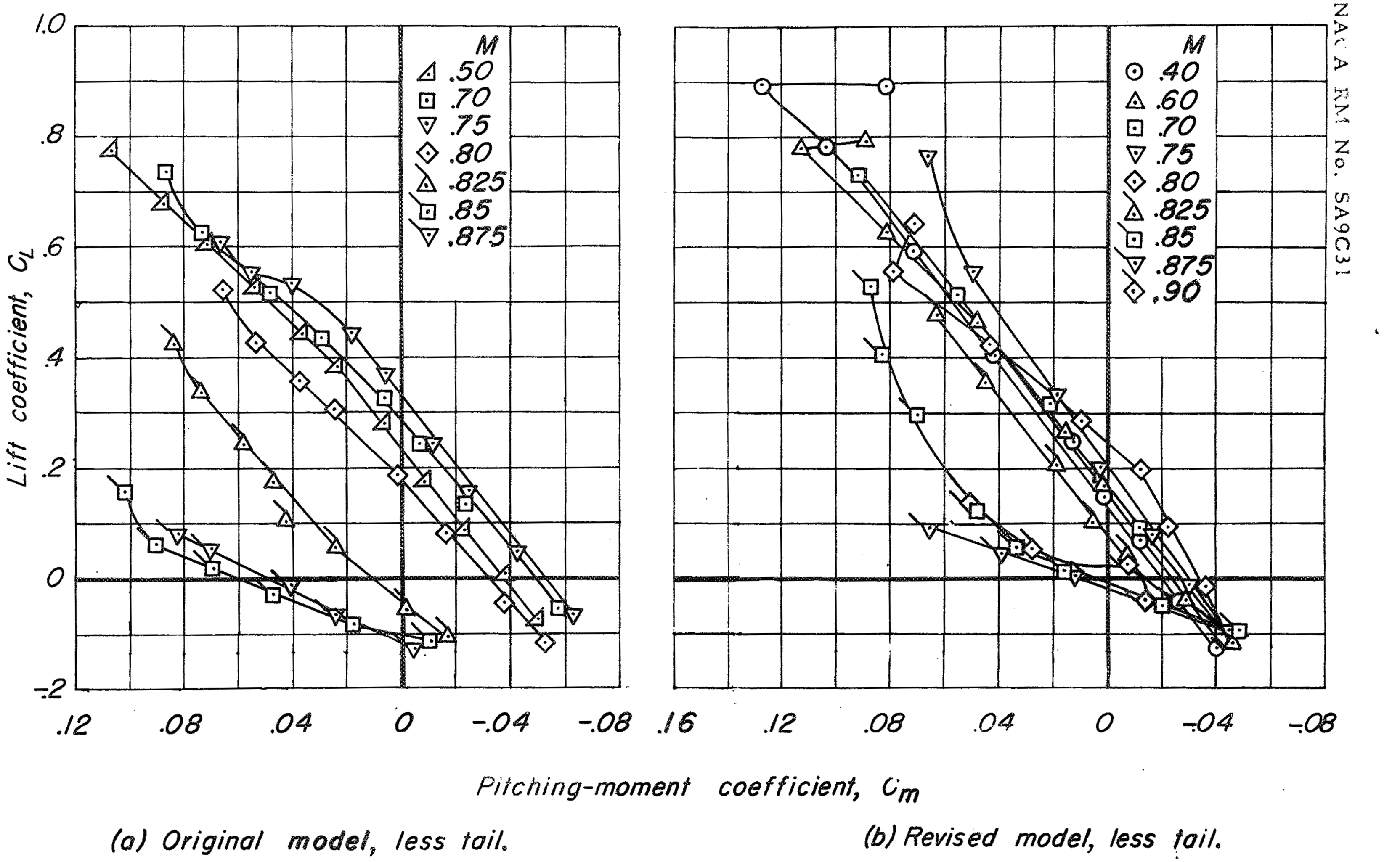

Figure 7.- Variation of pitching-moment coefficient with lift coefficient at various Mach numbers for the original and revised models, with and without tail surfaces.

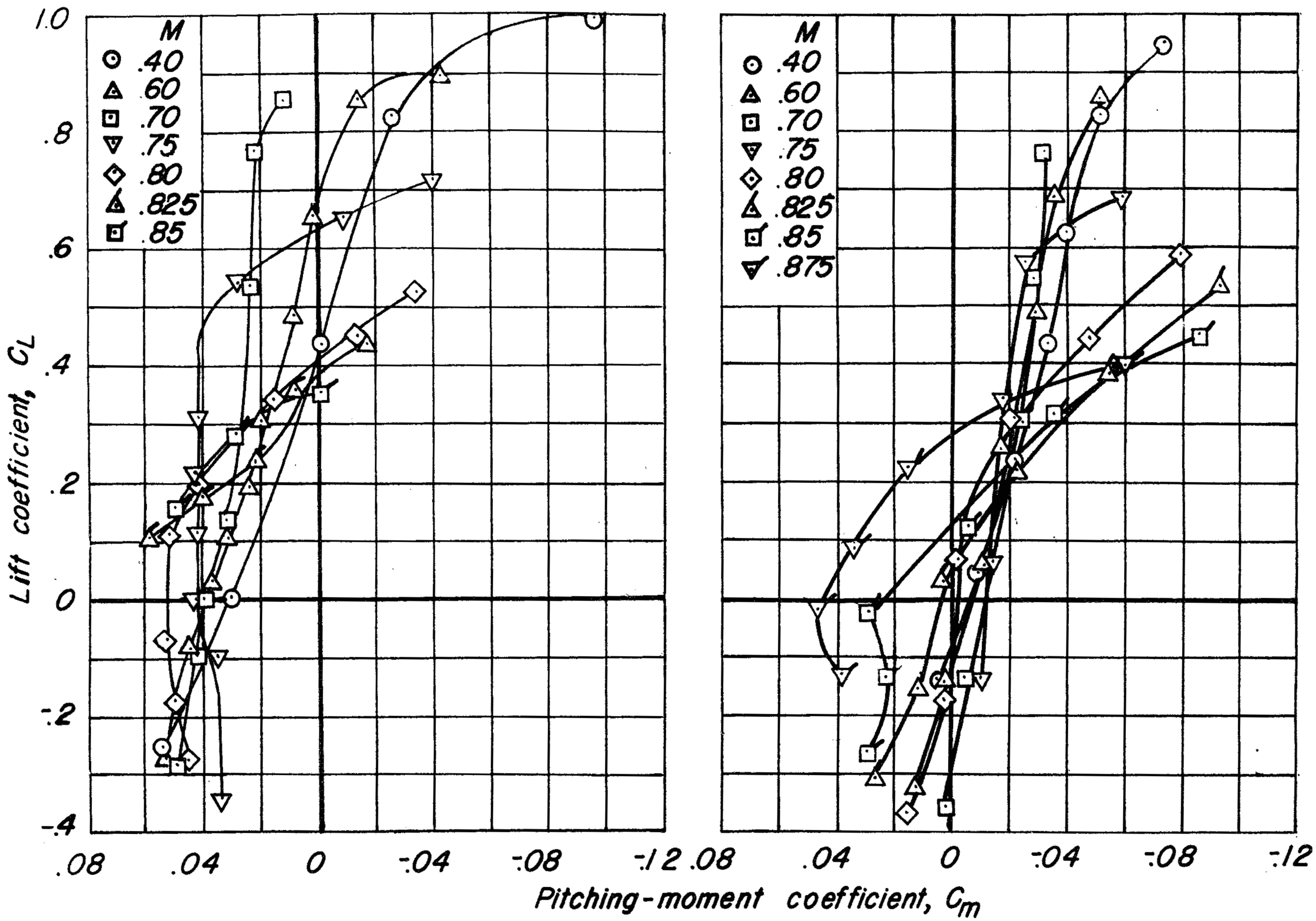

(c) Original model. i_t, 0°

(d) Revised model. i_t, 1°

Figure 7.- Concluded.

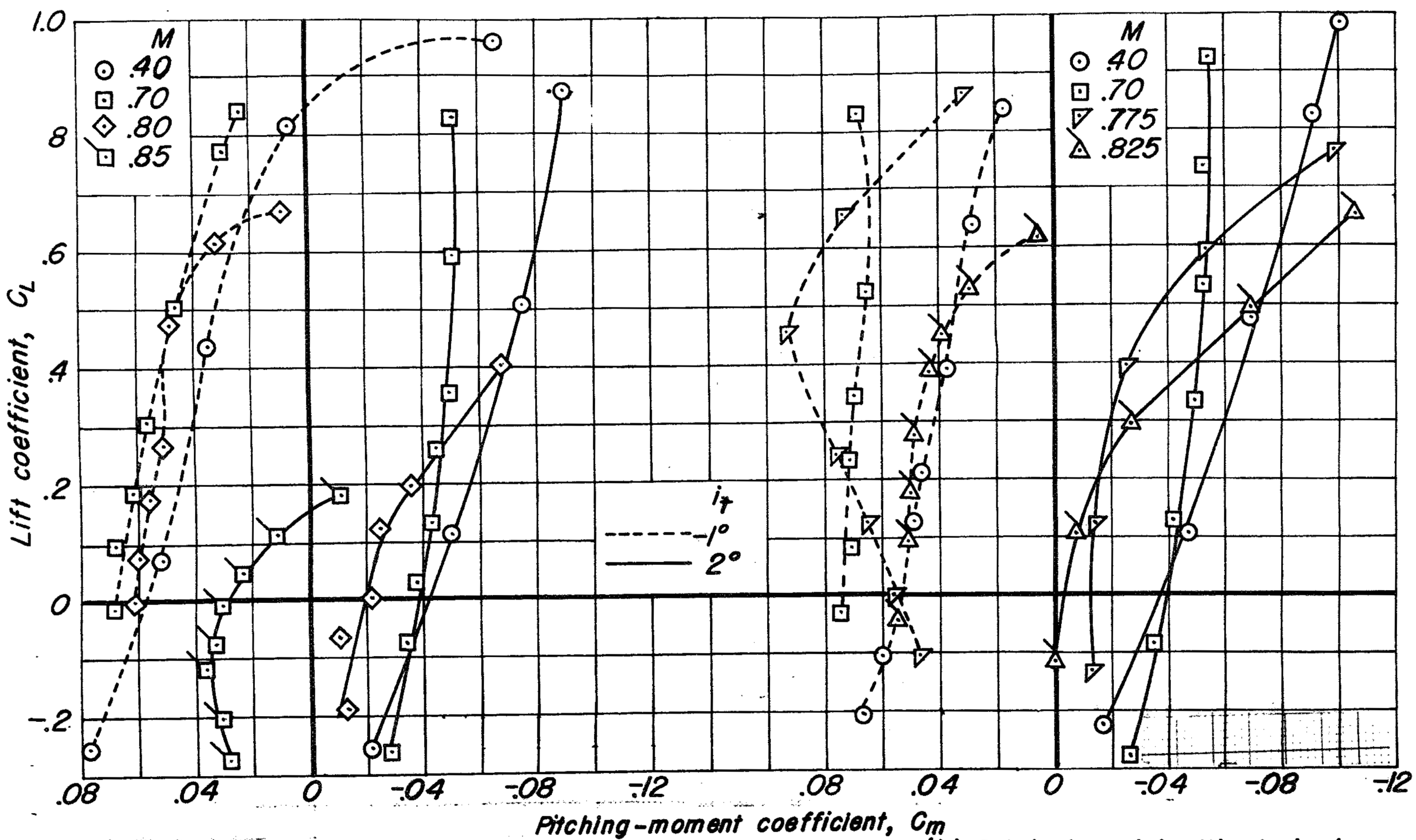

(a) Original model.

(b) Original model with air brakes.

Figure 8.- Effect of Mach number and stabilizer incidence on the variation of pitching-moment coefficient with lift coefficient for the original model, with and without air brakes. Elevators neutral.

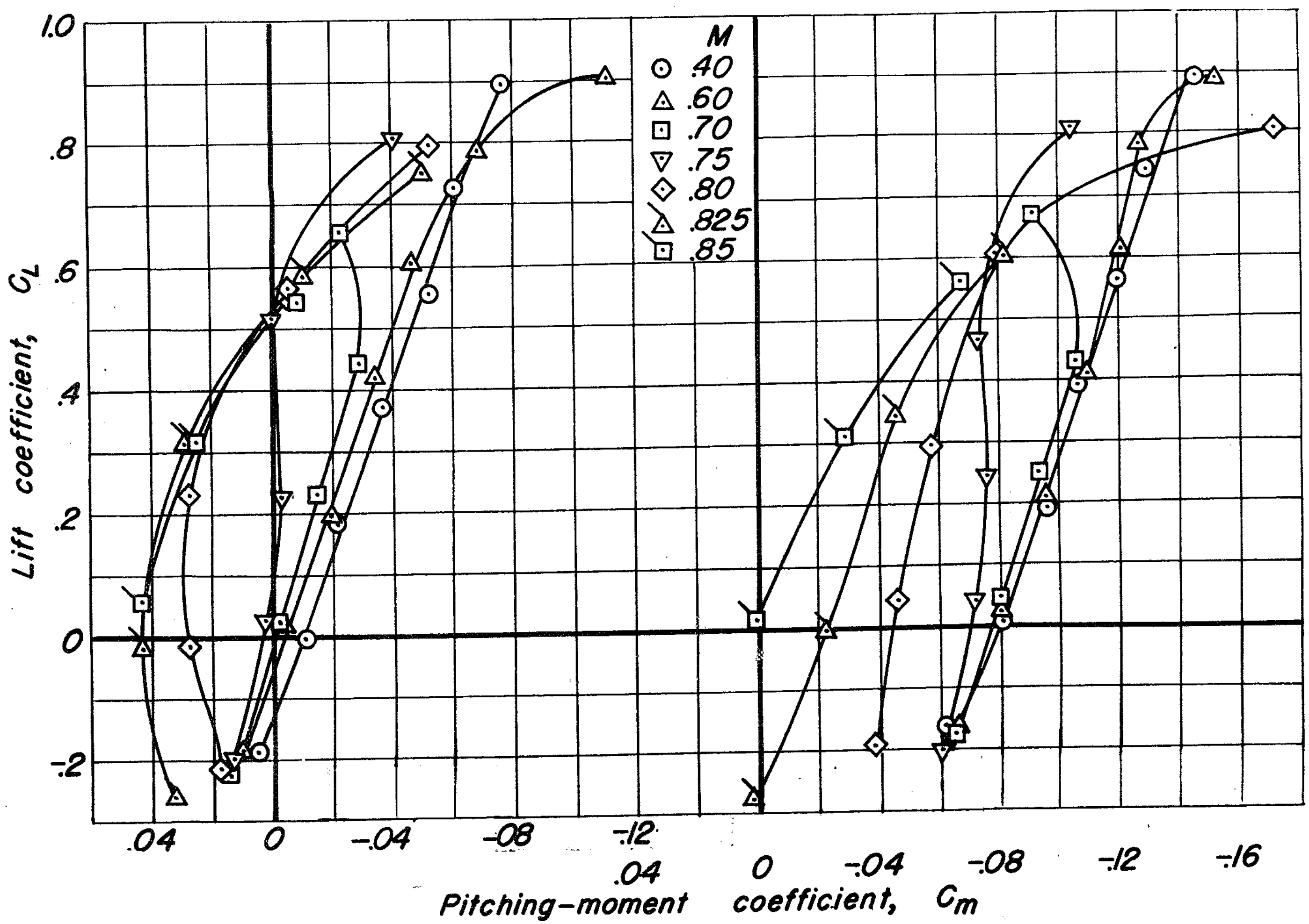

(a) δ_e, 0°.

(b) δ_e, 4°.

Figure 9.- Variation of pitching-moment coefficient with lift coefficient at various Mach numbers for the revised model with airbrakes.

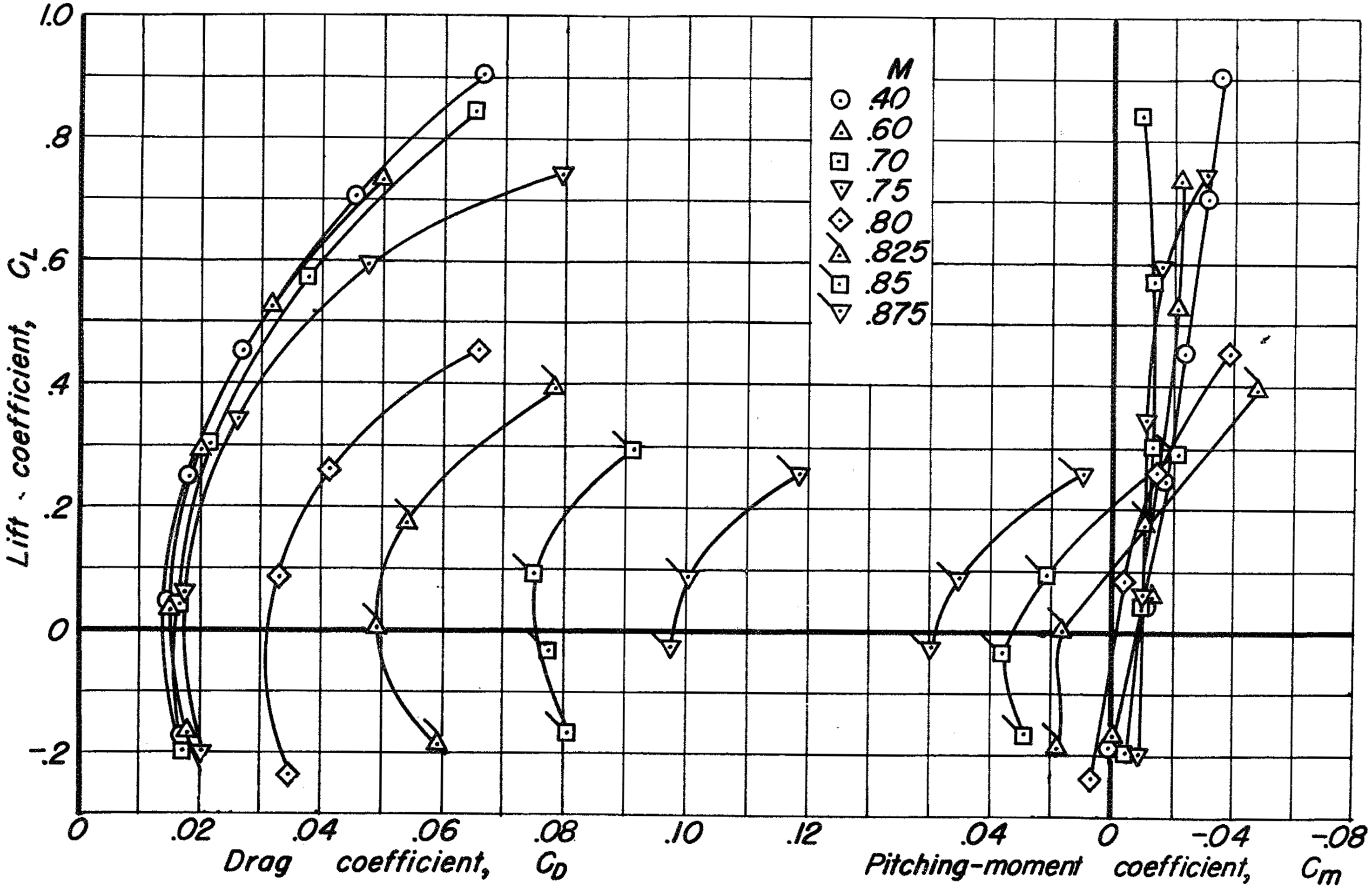

Figure 10.- Variation of drag and pitching-moment coefficients with lift coefficient at various Mach numbers for the revised model with wing-tip tanks. Elevators neutral.

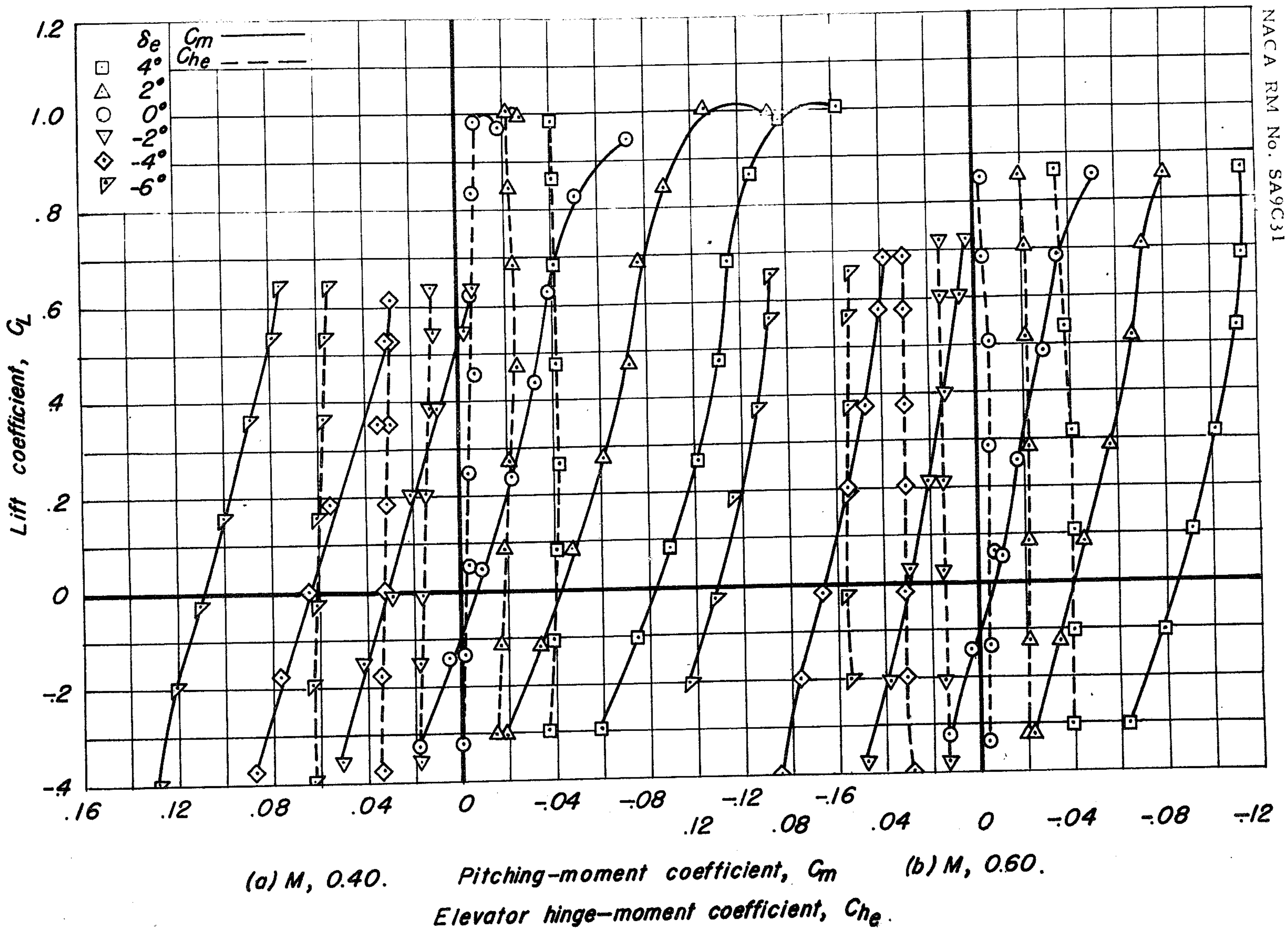

Figure 11.- Variation of pitching-moment and elevator hinge-moment coefficients with lift coefficient at various Mach numbers for the revised model.

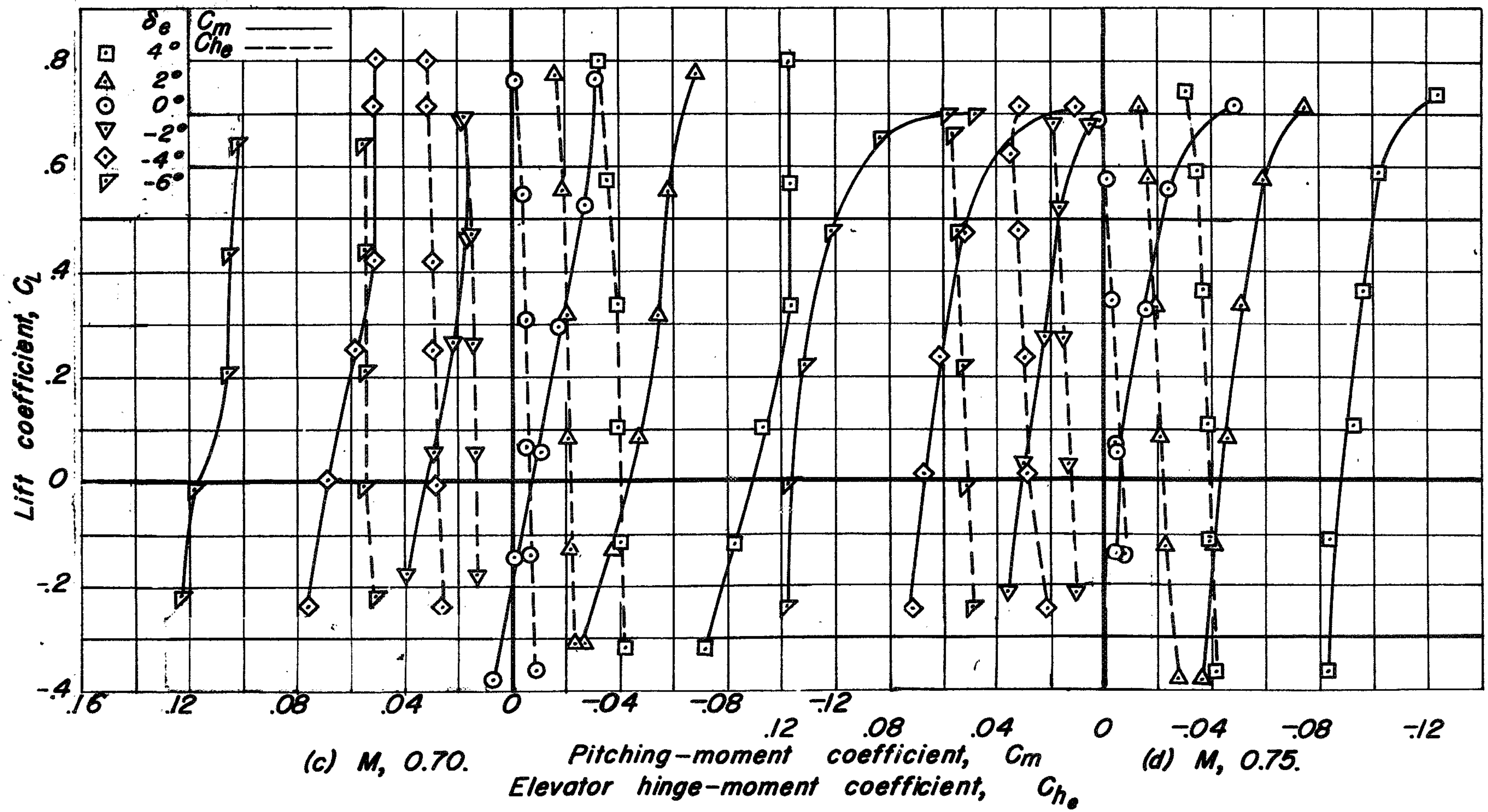

Figure 11.- Continued.

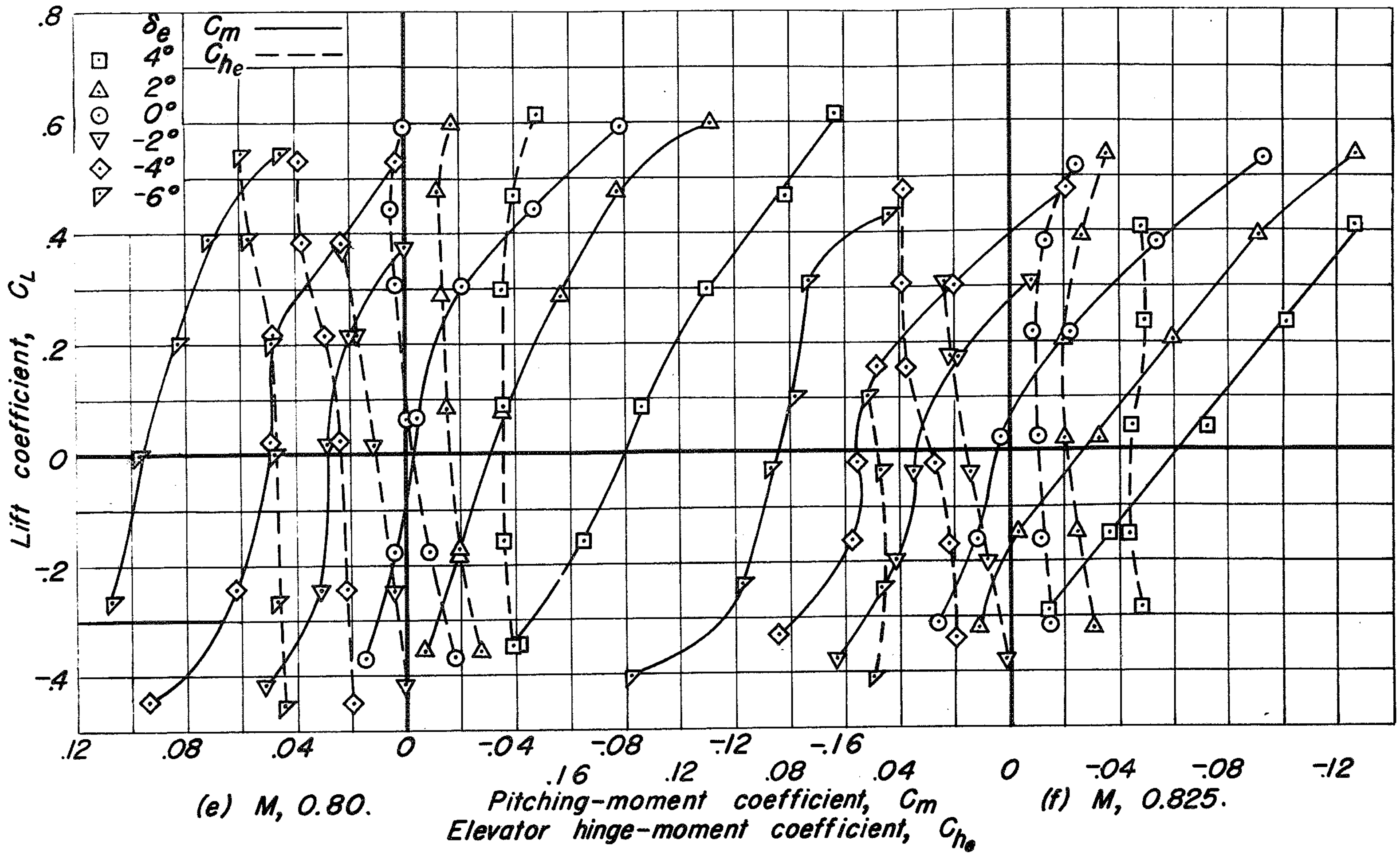

Figure 11.- Continued.

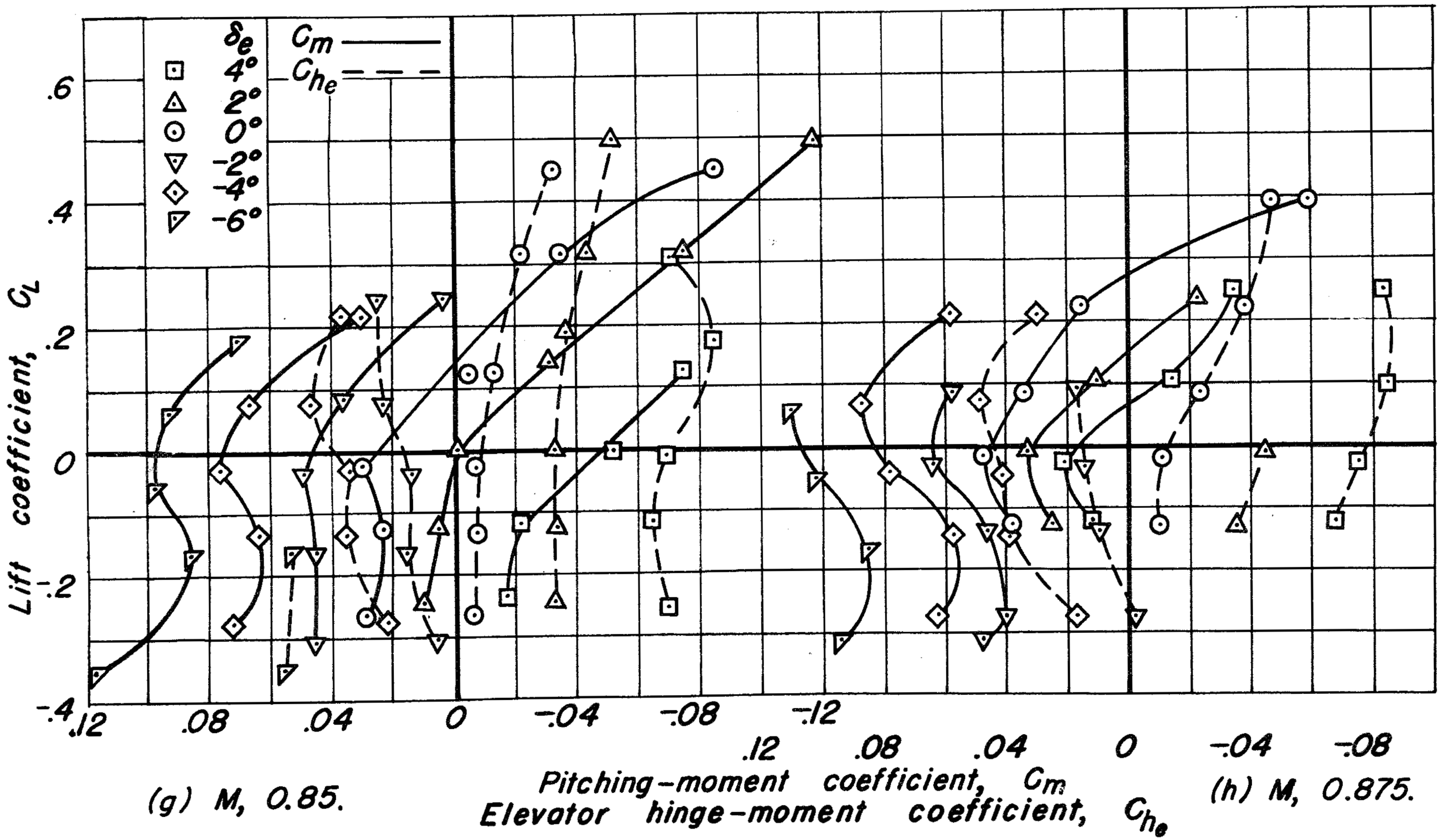

Figure 11.- Concluded.

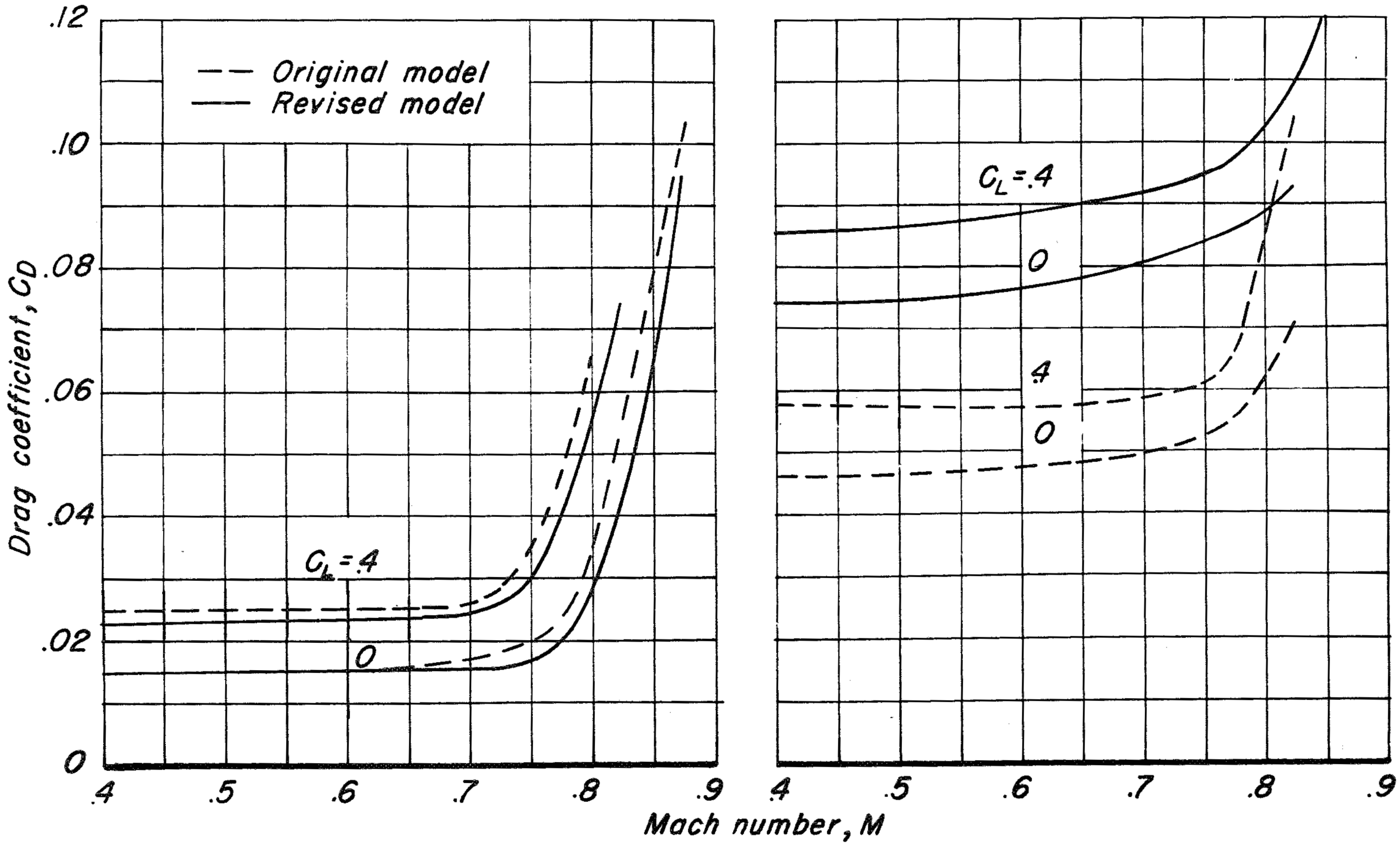

(a) Model without air brakes.

(b) Model with air brakes.

Figure 12.– Variation with Mach number of the drag coefficients for the original and revised models with and without air brakes.

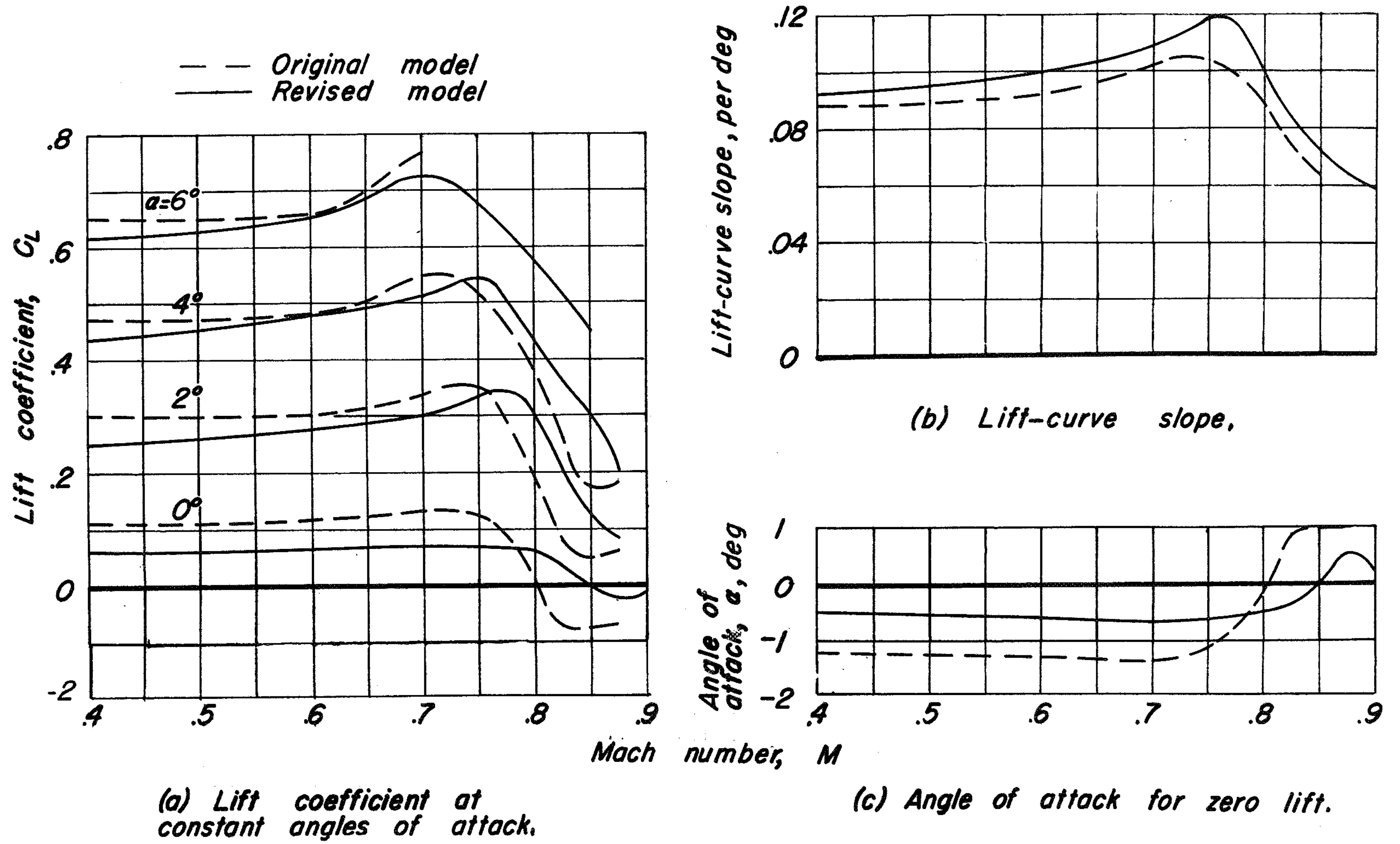

Figure 13.- Variation with Mach number of several aerodynamic parameters for the original and revised models.

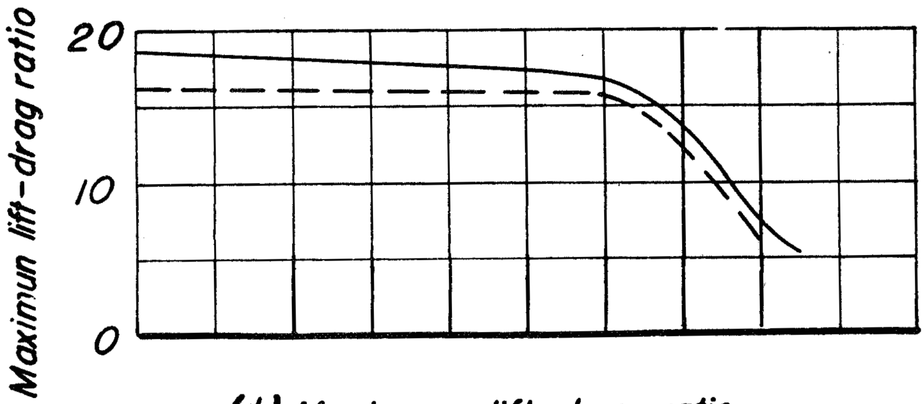

(d) Maximum lift-drag ratio.

- - - - Original model
——— Revised model

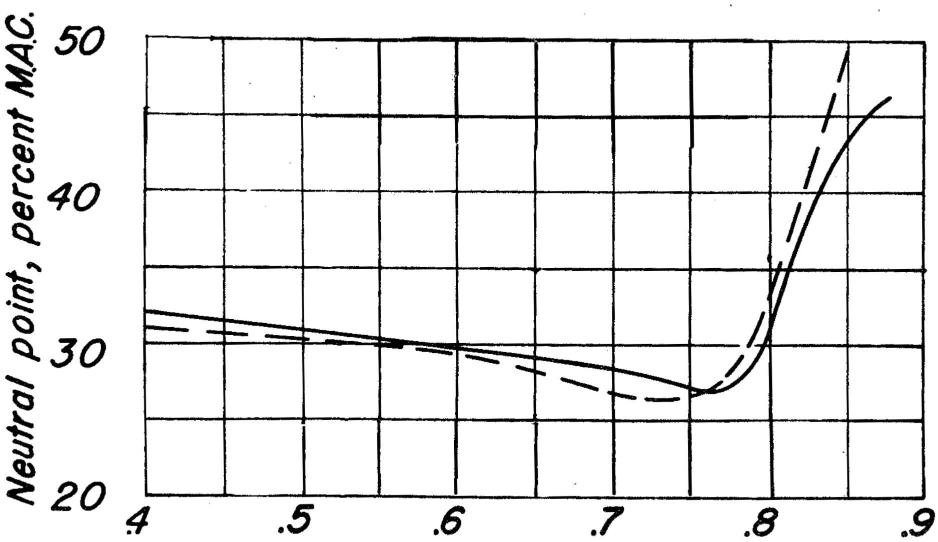

(e) Stick-fixed neutral point. C_L, 0.1.

Figure 13.- Continued.

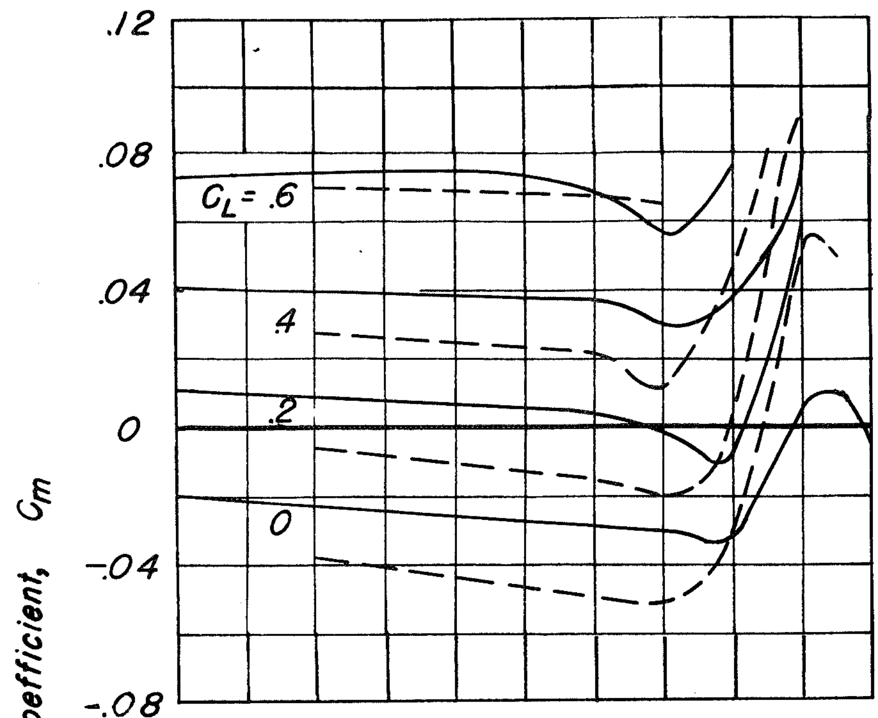

(f) Pitching-moment coefficient with tail surfaces removed.

– – – – Original model
———— Revised model

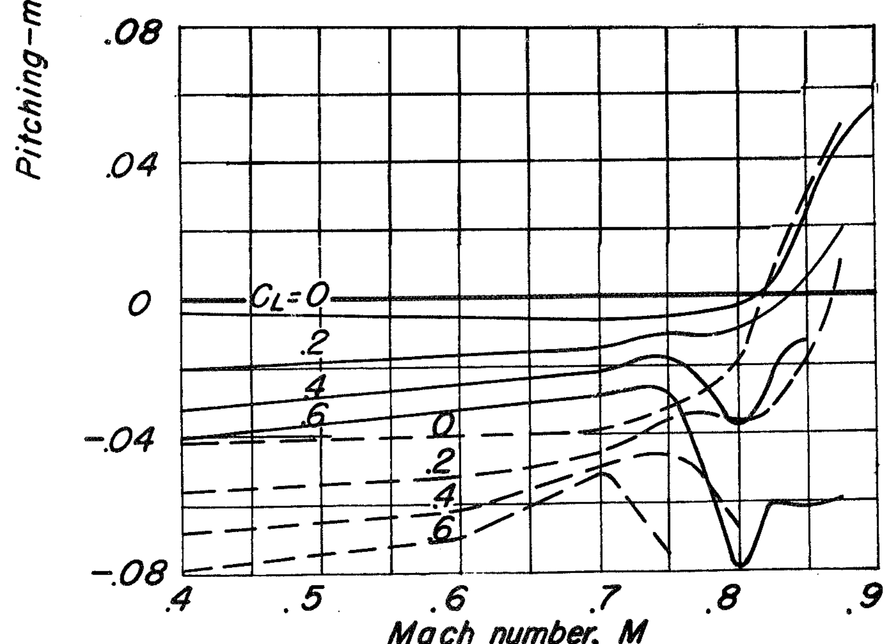

(g) Pitching-moment coefficient for complete model.

Figure 13.- Continued.

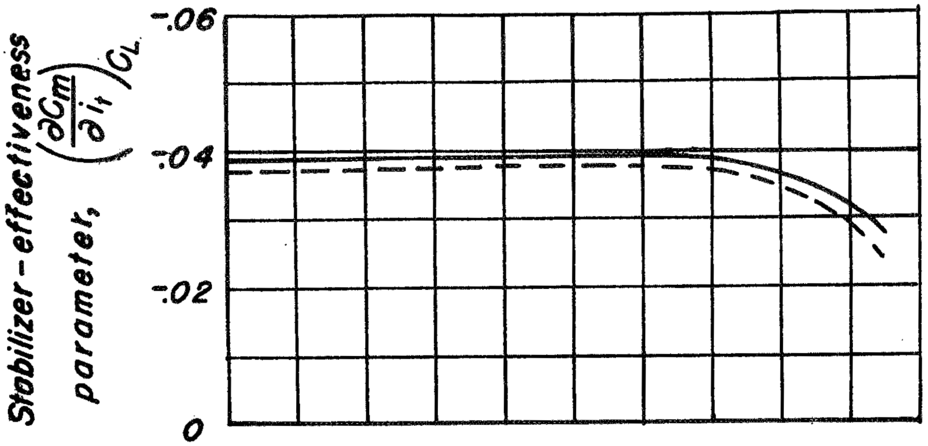

(h) Stabilizer-effectiveness parameter.

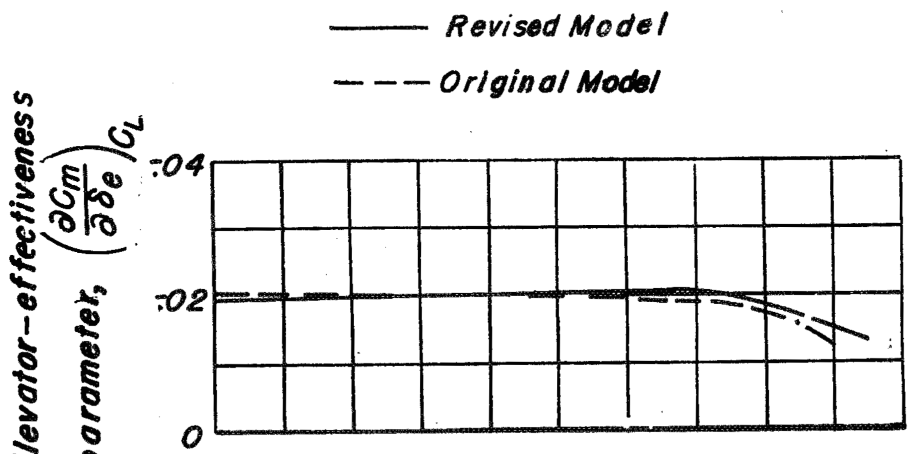

(i) Elevator-effectiveness parameter.

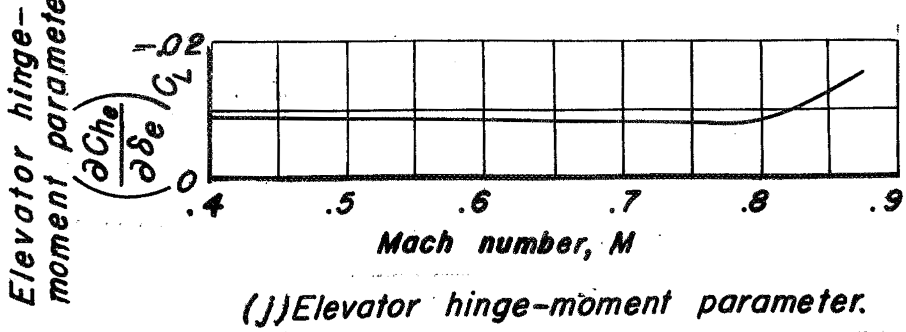

(j) Elevator hinge-moment parameter.

Figure 13.- Concluded.

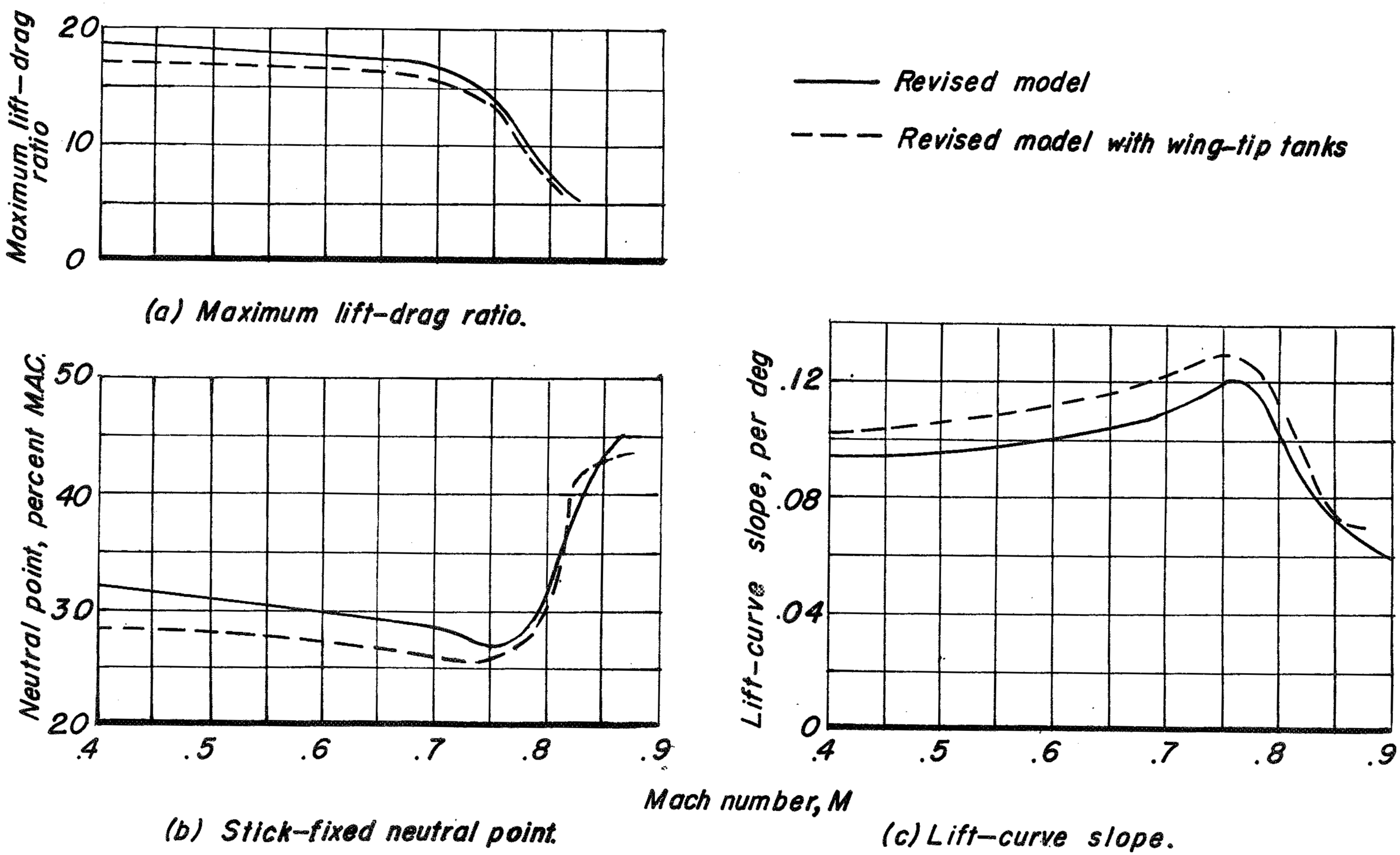

Figure 14.- Variation with Mach number of the stability and performance parameters for the revised model with and without wing-tip tanks.

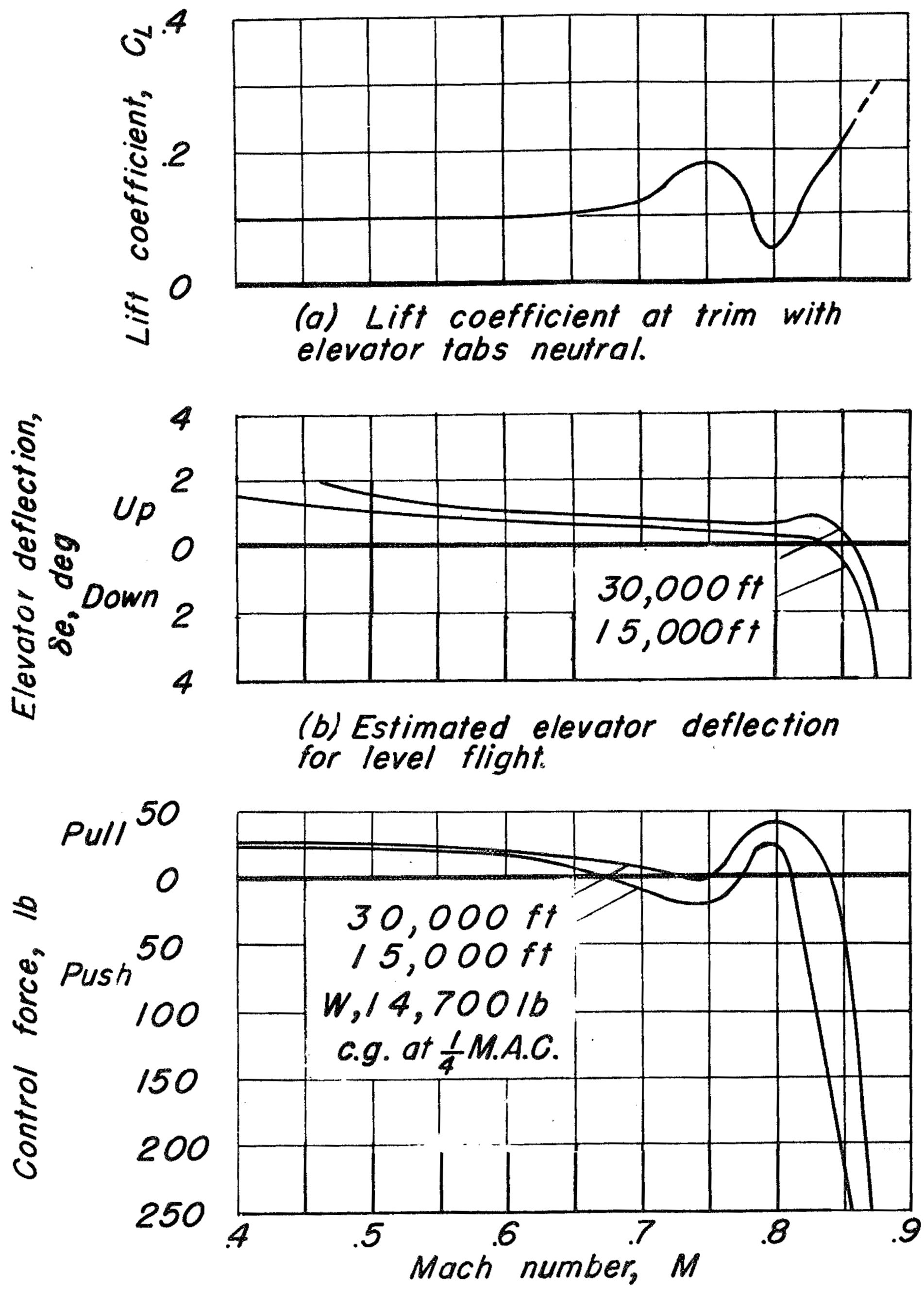

(a) Lift coefficient at trim with elevator tabs neutral.

(b) Estimated elevator deflection for level flight.

(c) Calculated control force for level flight. Tabs neutral; stick length, 1.87 feet.

Figure 15.- Variation with Mach number of the trim lift coefficient with elevators neutral and of the estimated elevator deflections and longitudinal control forces required for level flight. i_t, 1.°

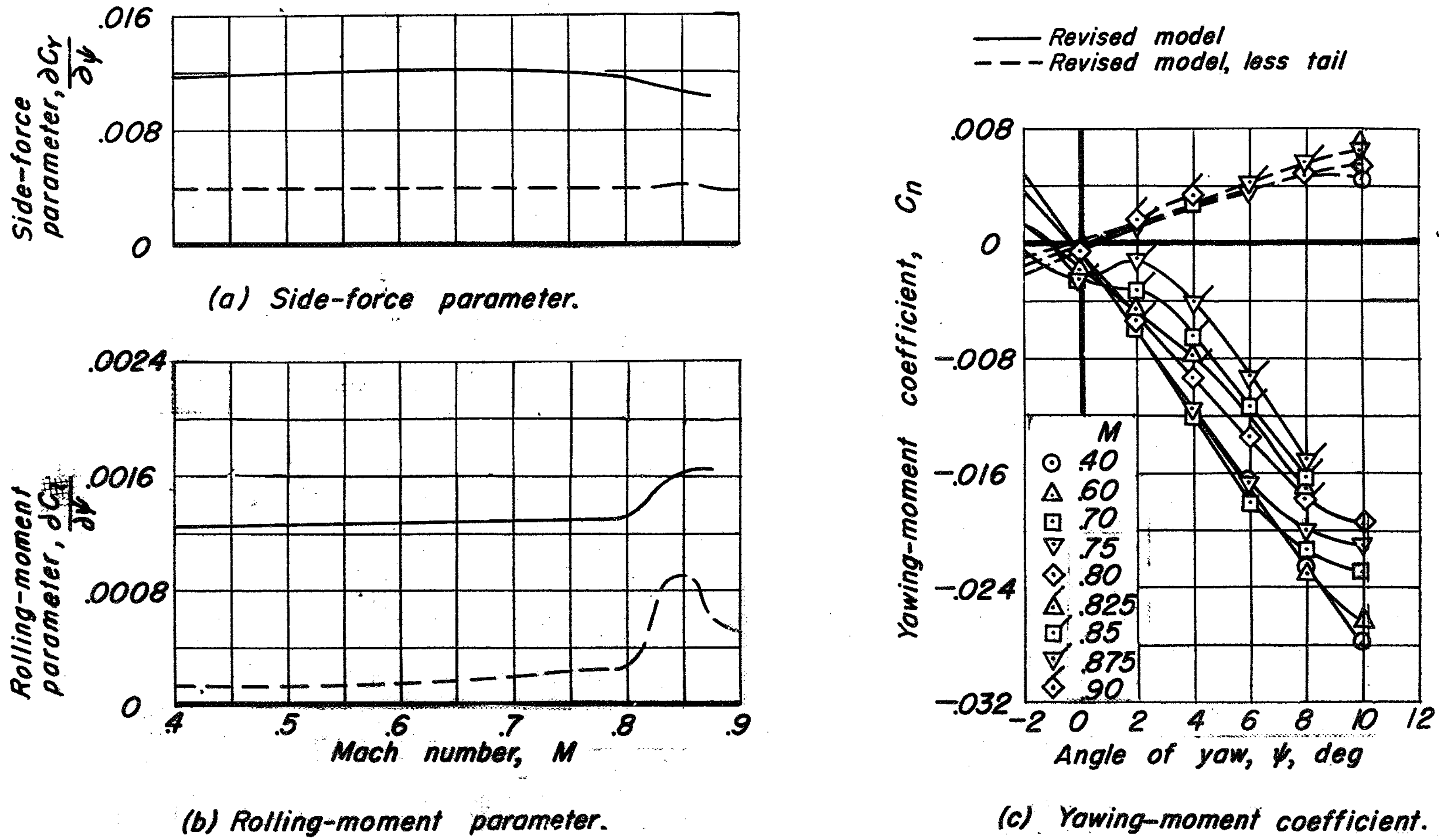

Figure 16.- Variation with Mach number of the directional-stability parameters for the revised model. $\alpha, 0^\circ; \delta_r, 0^\circ$.

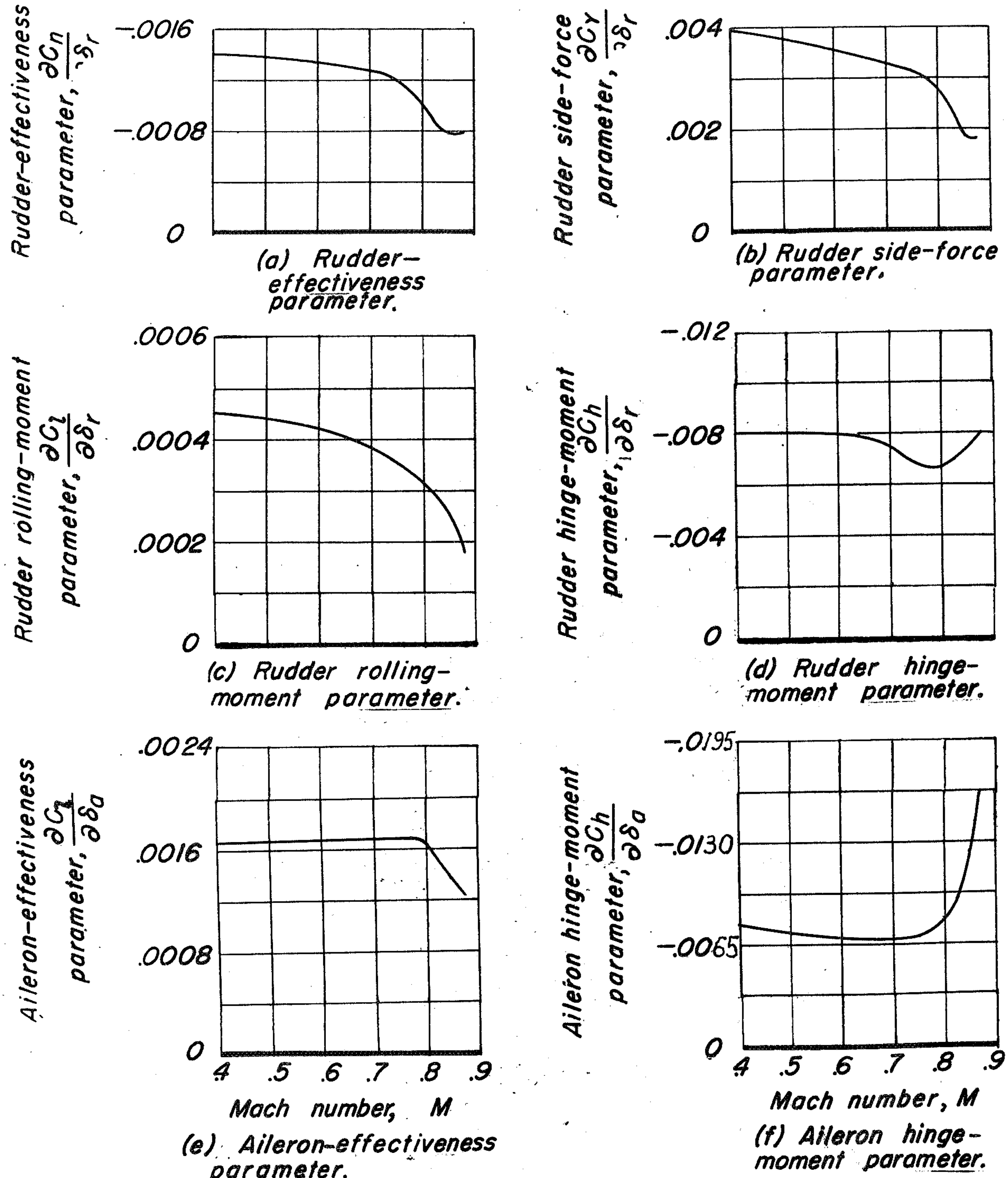

Figure 17.- Variation with Mach number of several rudder and aileron parameters for the revised model.

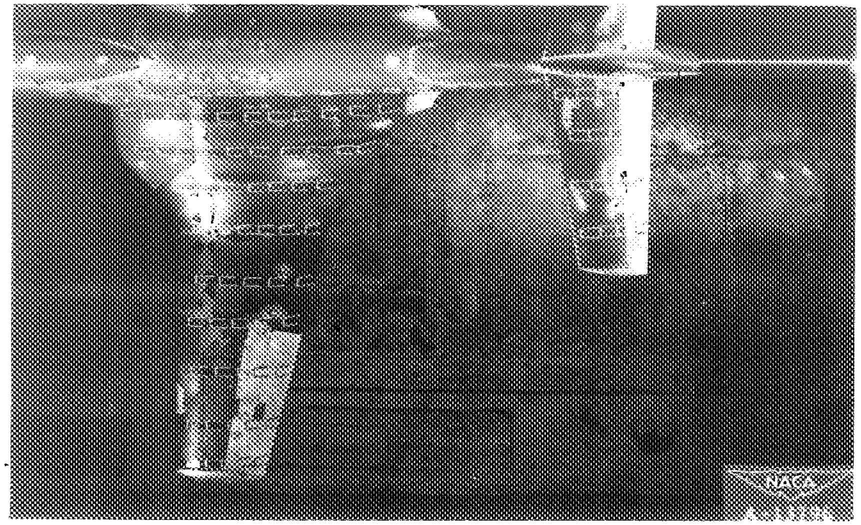

(a) Plan view. M, 0.40; α_u, 0°; C_L, 0.08.

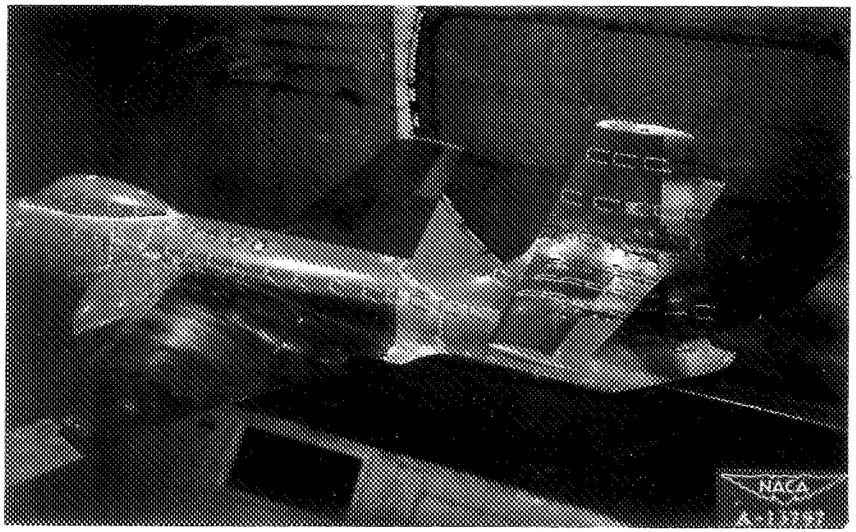

(b) Side view. M, 0.40; α_u, 0°; C_L, 0.08.

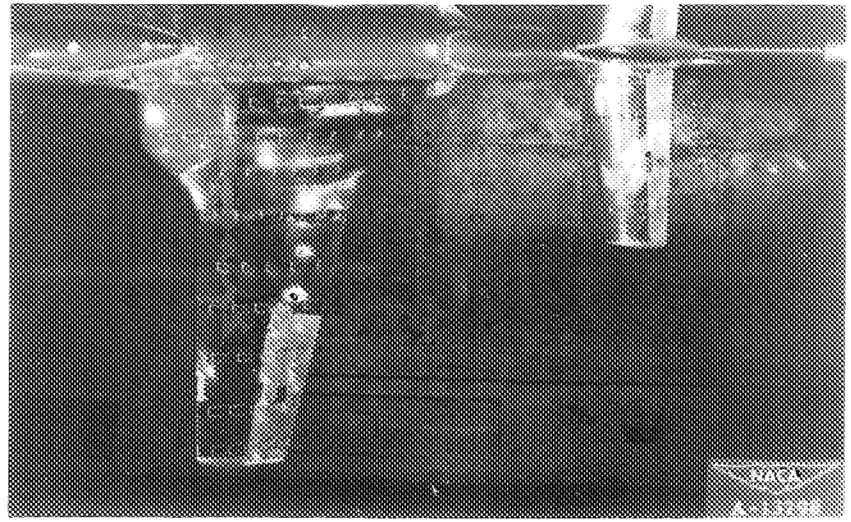

(c) Plan view. M, 0.40; α_u, 12°; C_L, 1.01.

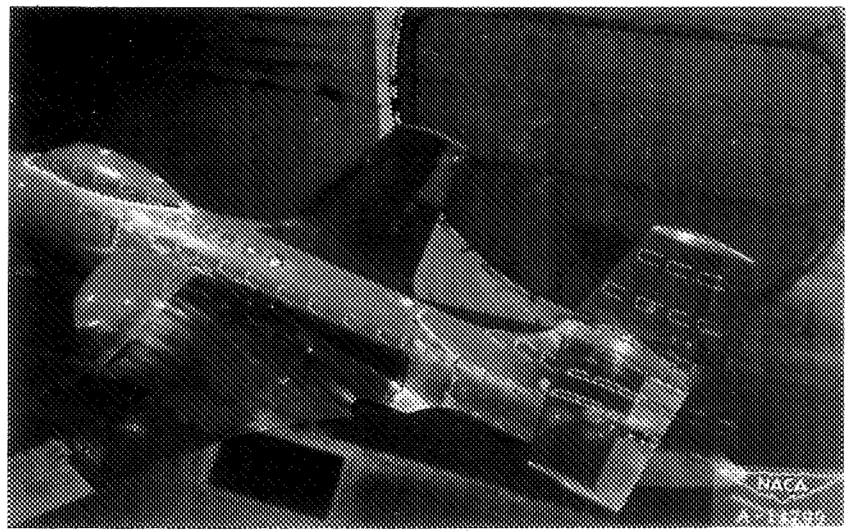

(d) Side view, M, 0.40; α_u, 12°; C_L, 1.01.

Figure 18.– Tufts on the original model.

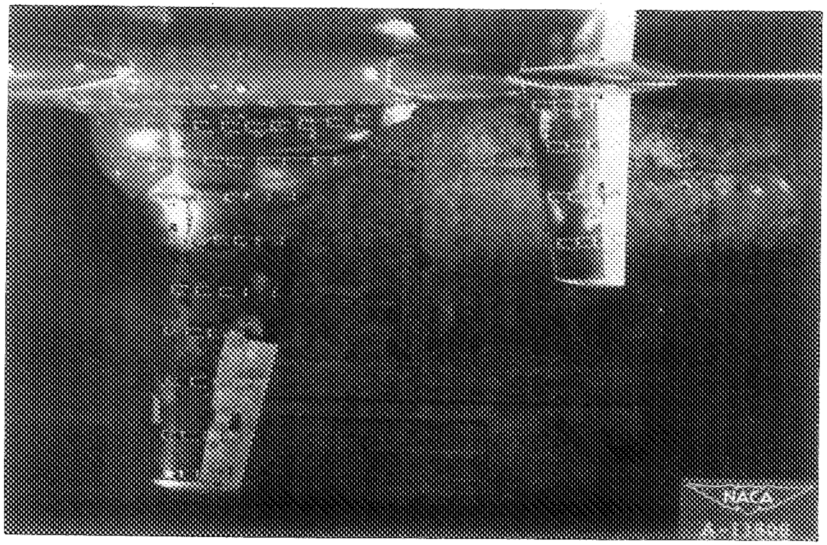

(e) Plan view, M, 0.825; α_u, 0°; C_L, –0.08.

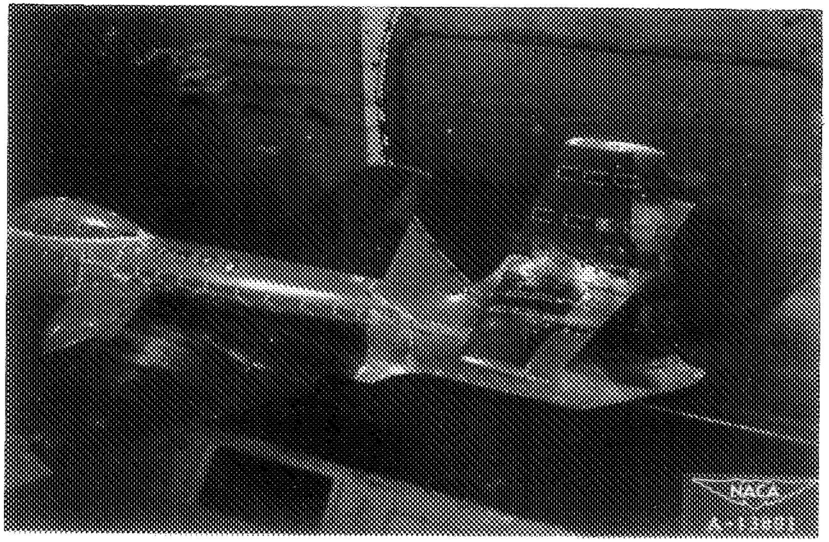

(f) Side view. M, 0.825; α_u, 0°, C_L, –0.08.

(g) Plan view, M, 0.825; α_u, 4°; C_L, 0.26.

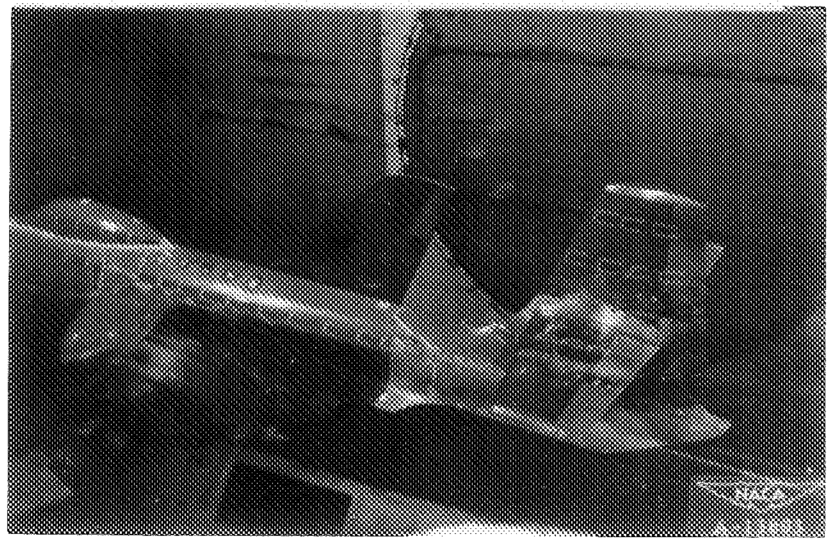

(h) Side view. M, 0.825; α_u, 4°; C_L, 0.26.

Figure 18.– Concluded.

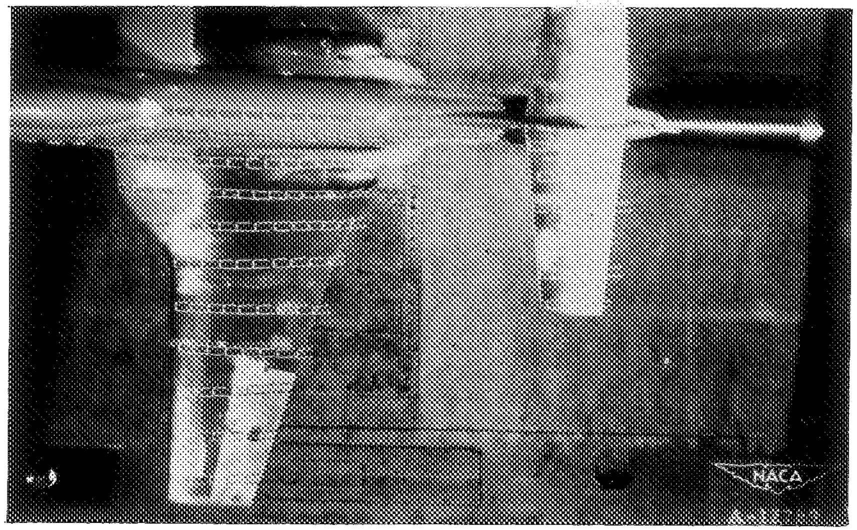

(a) Plan view. M, 0.40; α_u, 0°; C_L, 0.05.

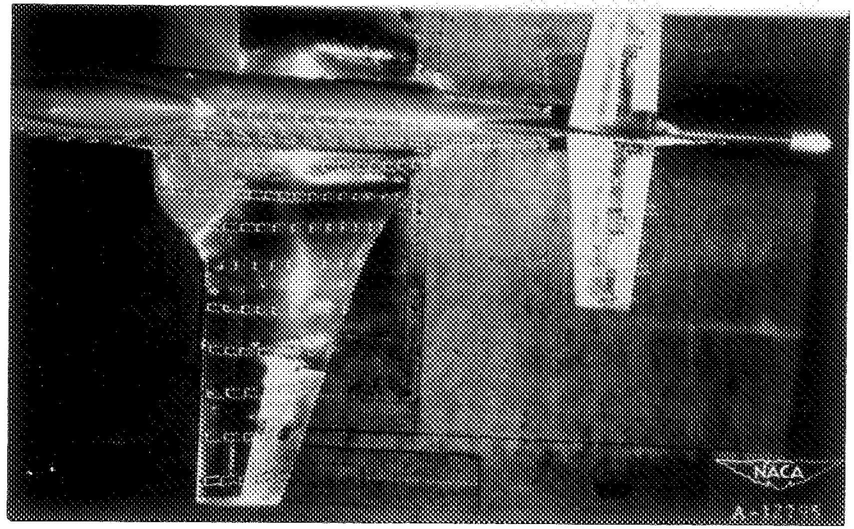

(c) Plan view. M, 0.40; α_u, 12°; C_L, 0.99.

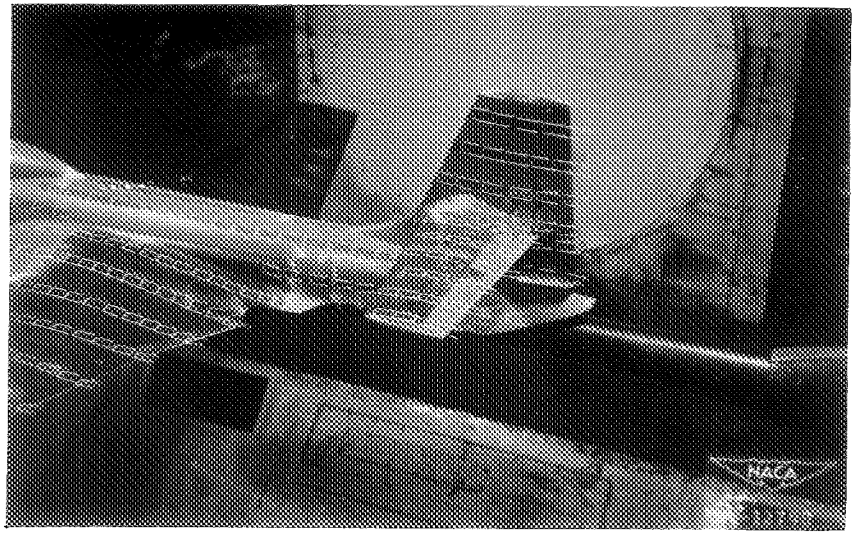

(b) Side view. M, 0.40; α_u, 0°; C_L, 0.05.

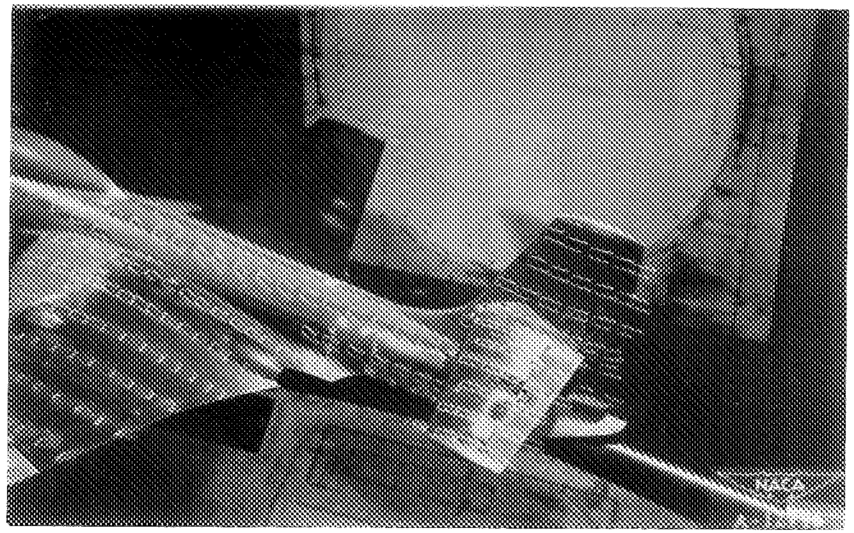

(d) Side view. M, 0.40; α_u, 12°; C_L, 0.99.

Figure 19.– Tufts on the revised model.

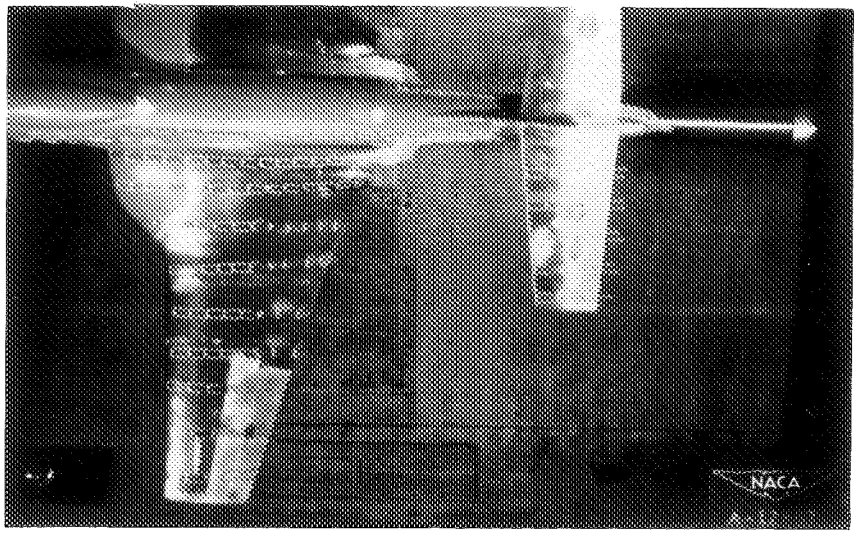

(e) Plan view, M, 0.825; α_u, 0°; C_L, 0.03.

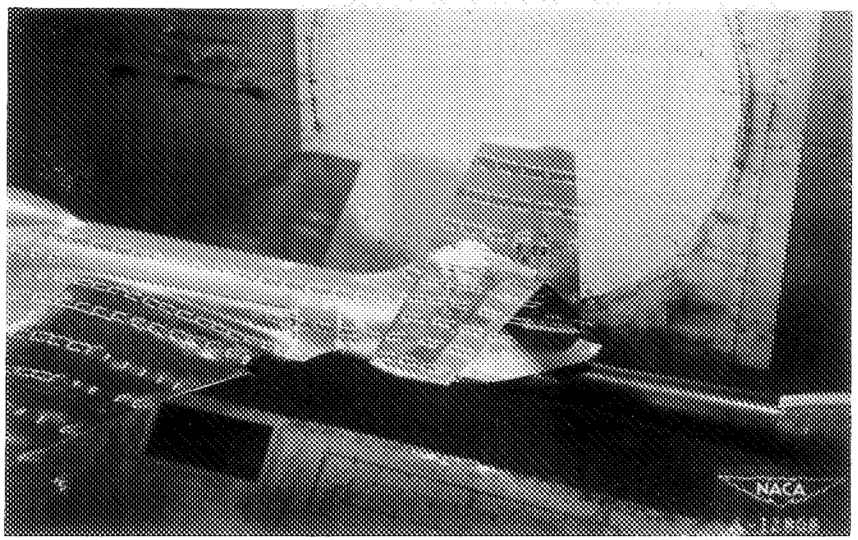

(f) Side view. M, 0.825; α_u, 0°; C_L, 0.03.

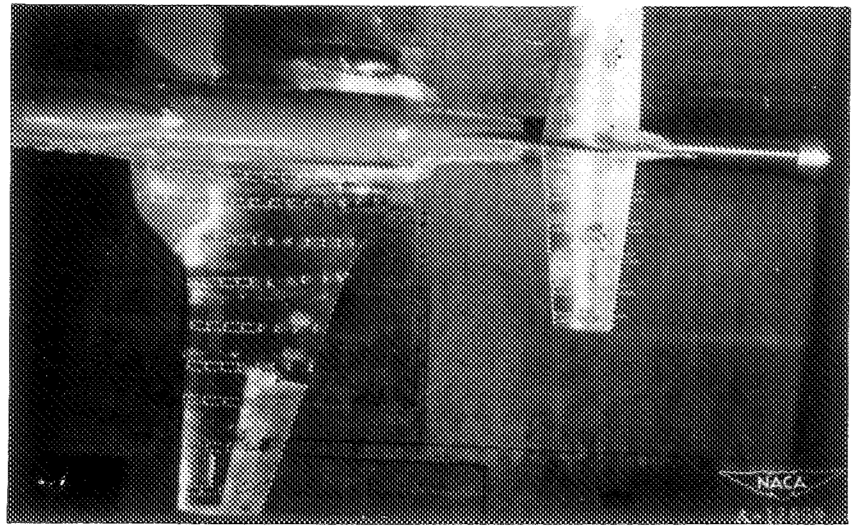

(g) Plan view. M, 0.825; α_u, 4°; C_L, 0.36.

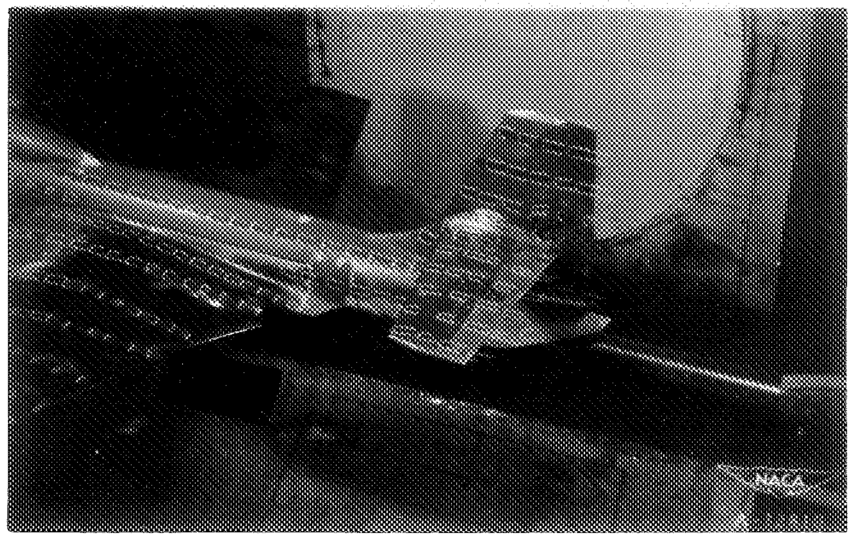

(h) Side view. M, 0.825; α_u, 4°; C_L, 0.36.

Figure 19.– Continued.

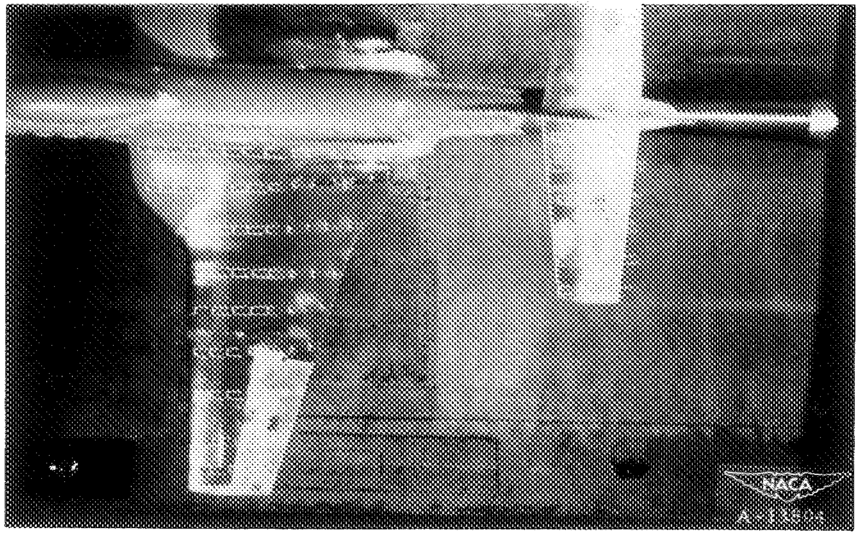

(i) Plan view. M, 0.875; α_u, 2°; C_L, 0.08.

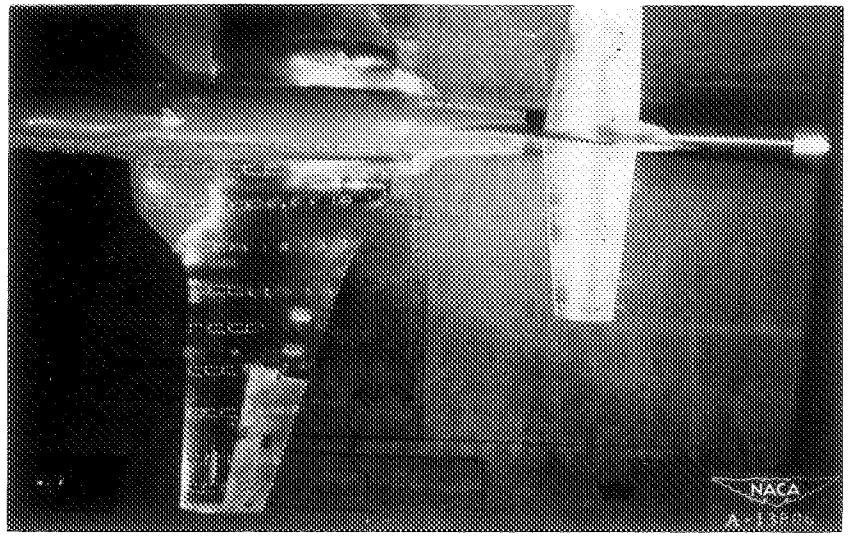

(k) Plan view.
M, 0.875; α_u, 6°; C_L, 0.3 (estimated)

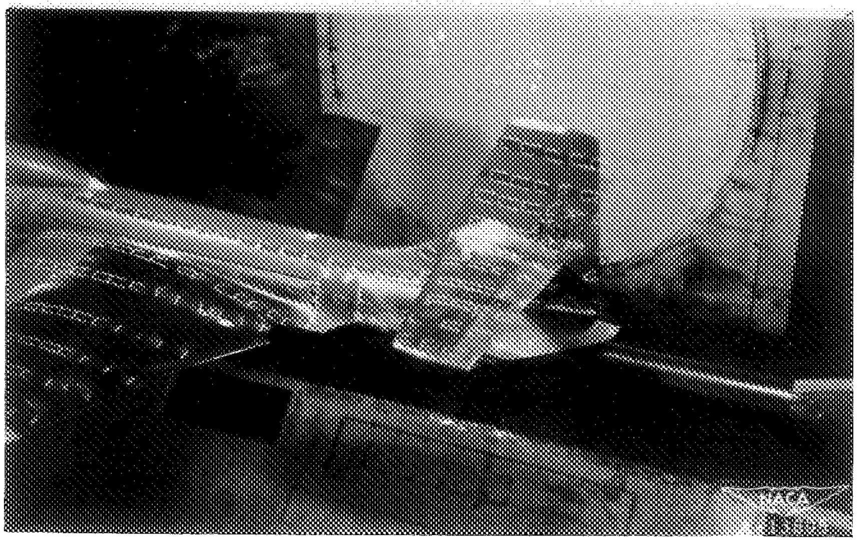

(j) Side view. M, 0.875; α_u, 2°; C_L, 0.08

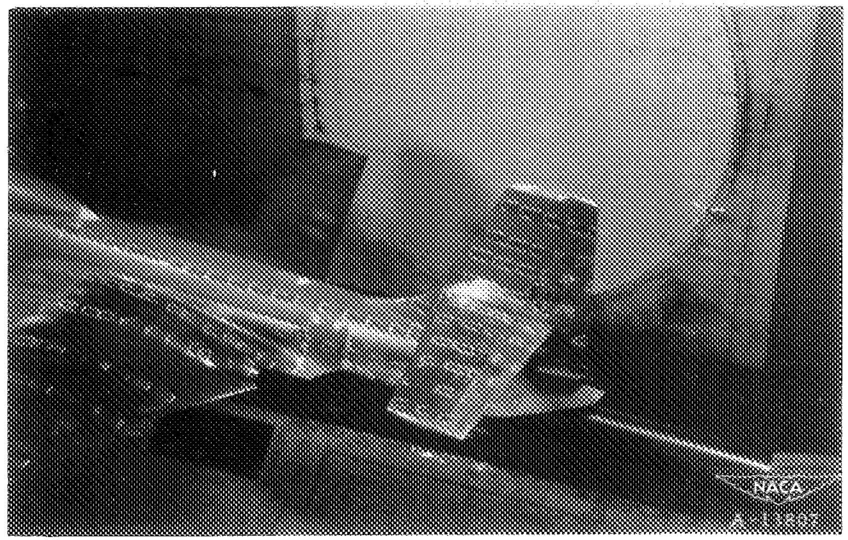

(l) Side view.
M, 0.875; α_u, 6°; C_L, 0.3 (estimated)

Figure 19.– Concluded.

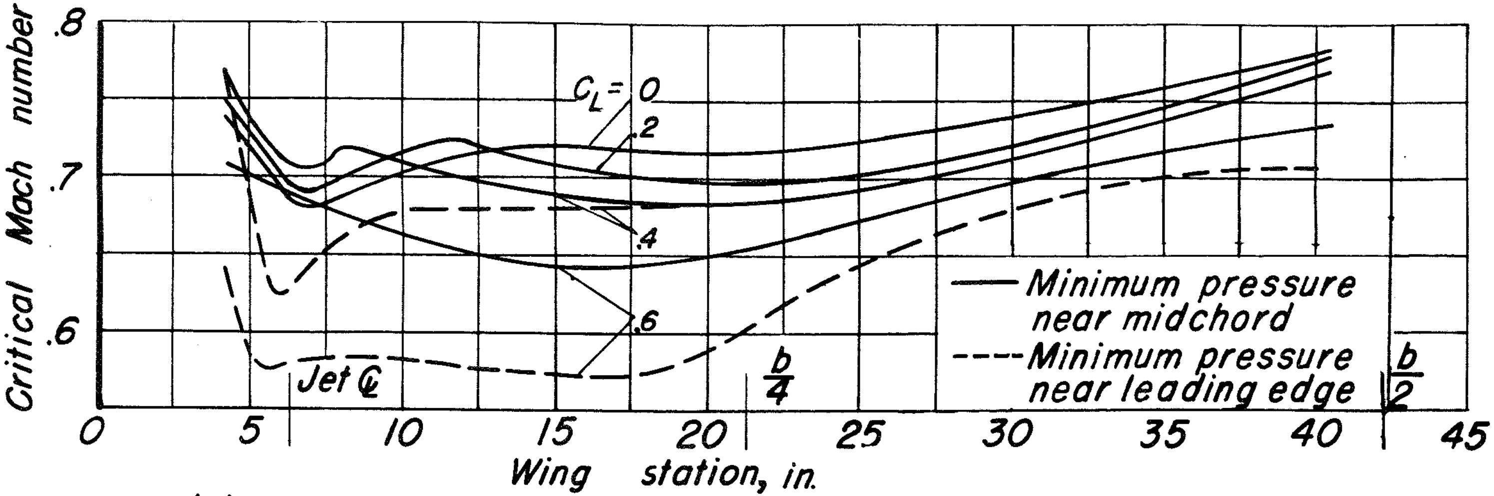

(a) Spanwise variation of critical Mach number for wing.

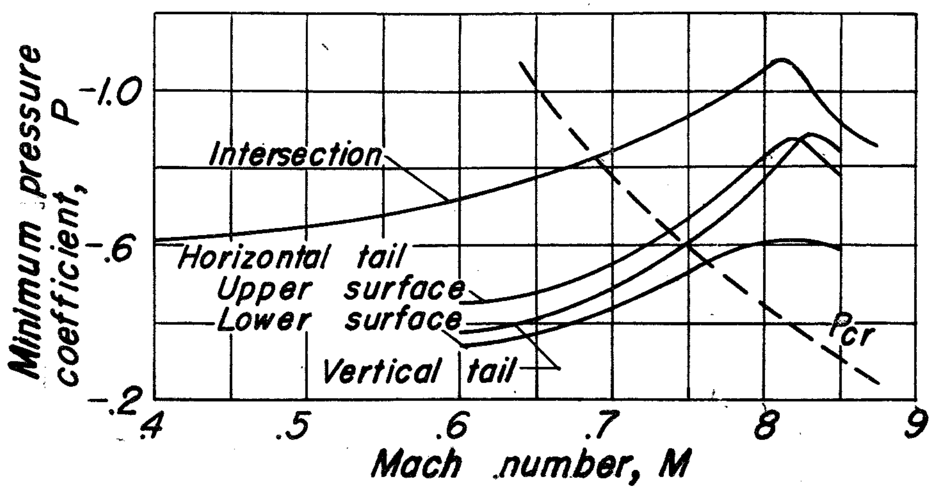

(b) Variation with Mach number of minimum pressure coefficient for the tail. Model lift coefficient, 0.2.

Figure 20.- Experimentally determined critical Mach number for the revised model.

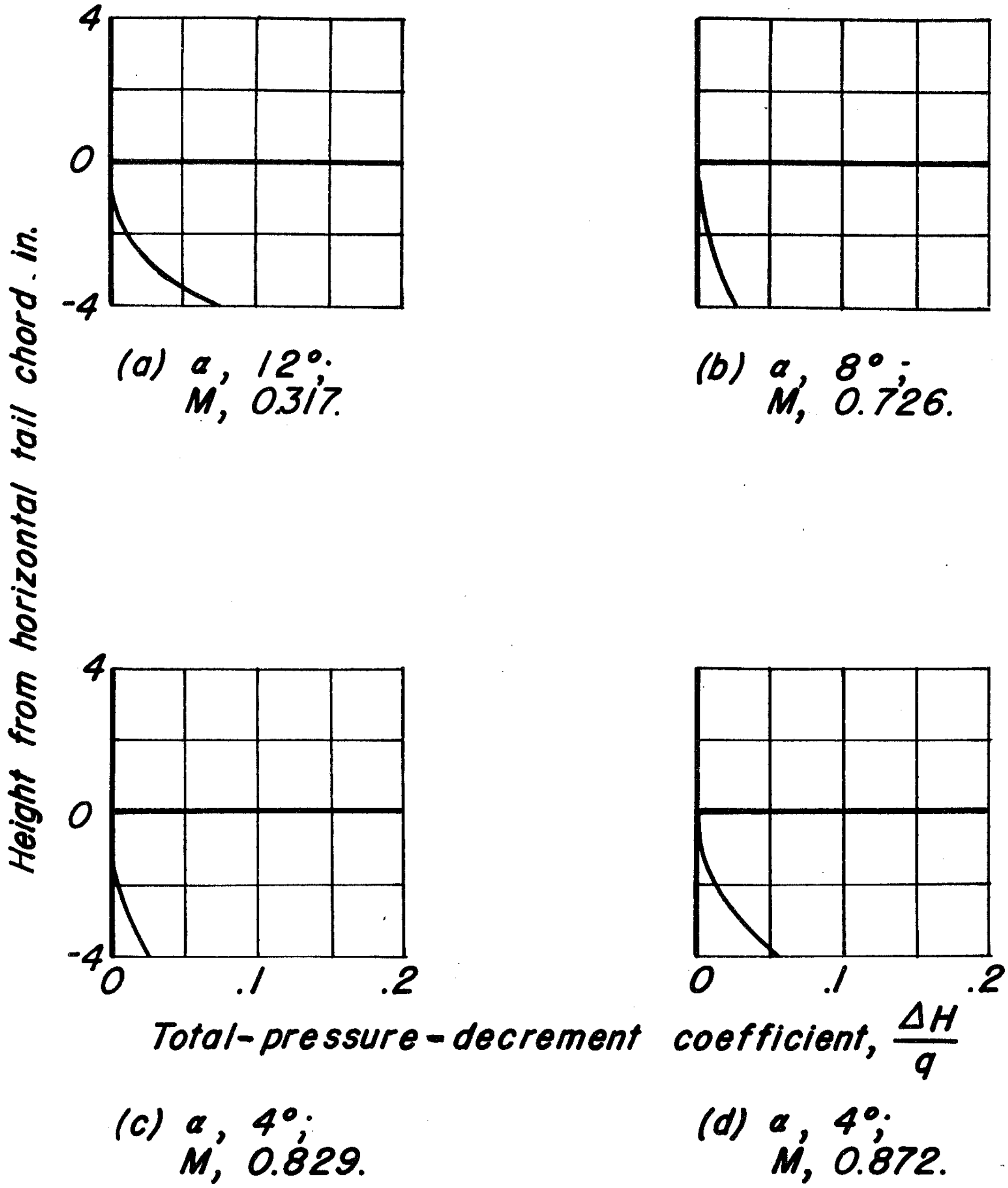

Figure 21.– Wing wake at leading edge of the horizontal tail measured at stabilizer station 6.3 inches.